Combination of CDF's searches for the standard model Higgs boson with up to 10.0 fb⁻¹ of data

The CDF Higgs Discovery Group

for the CDF Collaboration

March 6, 2012

We combine results from CDF's direct searches for the standard model (SM) Higgs boson (H) in $p\bar{p}$ collisions at the Fermilab Tevatron at $\sqrt{s}=1.96$ TeV. Compared to the previous Tevatron Higgs search combination, $\sim 20\%$ more integrated luminosity have been added, and we achieve gains in expected sensitivity beyond luminosity of 12 % due mainly to a new algorithm to identify b-quark jets. With up to 10.0 fb⁻¹ of integrated luminosity, the 95% C.L. upper limits on Higgs boson production are 2.17, 2.67 and 0.41 times the values of the SM cross section for Higgs boson masses of $m_H = 115 \text{ GeV}/c^2$, $m_H = 125 \text{ GeV}/c^2$, and 165 GeV/c^2 , respectively. The corresponding median upper limits expected in the absence of Higgs boson production are 1.18, 1.40, and 0.67. We exclude, at the 95% C.L., a new and larger region at high mass between 148.8 $< m_H < 175.2 \text{ GeV}/c^2$ and $90 < m_H < 96.9 \text{ GeV}/c^2$, with an expected exclusion region of $m_H < 94.2 \text{ GeV}/c^2$, $96.1 < m_H < 106 \text{ GeV}/c^2$ and $153.8 < m_H < 176.1 \text{ GeV}/c^2$. There is an excess of data events with respect to the background estimation in the mass range $100 < m_H < 145 \text{ GeV}/c^2$ which causes our limits to not be as stringent as expected. The largest excess at $m_H = 120 \text{ GeV}$ has a local p-value corresponding to a local significance of 2.6 σ . The global significance for such an excess anywhere in the full mass range is approximately 2.1 σ . We combine separately searches for $W/Z+H\to b\bar{b}$ and $H\to W^+W^-$, and find that the excess is concentrated in the $H \to b\bar{b}$ channel, where the local significance is 2.9 σ and the global signficance is 2.7 σ . The excess in our $H \to b\bar{b}$ channels has the highest global significance for a Higgs signal achieved to date from a Tevatron or LHC experiment.

Preliminary Results

I. INTRODUCTION

The search for a mechanism for electroweak symmetry breaking, and in particular for a standard model (SM) Higgs boson, has been a major goal of particle physics for many years, and is a central part of the Fermilab Tevatron physics program. Precision electroweak data, including the recently updated measurements of the W-boson mass from the CDF and D0 Collaborations [1, 2], yield an indirect constraint on the allowed mass of the Higgs boson, $m_H < 152 \text{ GeV}/c^2$ [3], at 95% confidence level (C.L.). The Large Electron Positron Collider (LEP) has excluded Higgs boson masses below 114.4 GeV/c^2 [4], and the LHC experiments, ATLAS and CMS, now limit the SM Higgs boson to have a mass between 115.5 and 127 GeV/c^2 [5, 6] at the 95% C.L. Both LHC experiments report local $\sim 3\sigma$ excesses at approximately 125 GeV/c^2 . We have updated our CDF searches for the SM Higgs boson, and a combination of these searches with those of D0 [7] is available in Ref. [8]. The new CDF searches include more data, the inclusion of additional channels, and improved analysis techniques compared to previous analyses. For searches in the $H \to b\bar{b}$ final state, substantial sensitivity gains were made by incorporating a new Neural Network b-quark jet tagging algorithm (HOBIT) [9]. The sensitivities of this new CDF combination exceeds those of previous CDF combinations and is comparable with the previous Tevatron combination [10, 11].

As a cross-check to establish the reliability of our analysis techniques, we use our analyses and combination machinery to measure WZ/ZZ production in final states with charged leptons and neutrinos and heavy flavor jets [12], and determine a 3.2 σ measurement of the cross section.

In this note, we combine the most recent results of all such searches in $p\bar{p}$ collisions at $\sqrt{s}=1.96$ TeV. The analyses combined here seek signals of Higgs bosons produced in association with vector bosons $(q\bar{q} \to W/ZH)$, through gluon-gluon fusion $(gg \to H)$, and through vector boson fusion (VBF) $(q\bar{q} \to q'\bar{q}'H)$ corresponding to integrated luminosities up to 10.0 fb⁻¹. In order to report an integrated luminosity corresponding to the data sample used to obtain our results, we average together the contributing searches' luminosities in a way that represents their contributions to the final results. A search with a low sensitivity contributes less to the average than searches with higher sensitivity. The overall sensitivity-weighted luminosities at low (< 135 GeV/ c^2) and high Higgs boson mass (> 135 GeV/ c^2) are 9.5 fb⁻¹ and 9.7 fb⁻¹, respectively. The Higgs boson decay modes studied are $H \to b\bar{b}$, $H \to W^+W^-$, $H \to Z^{\circ}Z^{\circ}$, $H \to \tau^+\tau^-$ and $H \to \gamma\gamma$.

To simplify the combination, the searches are separated into 91 mutually exclusive final states, which are listed in Table II, and which are referred to as "analysis sub-channels" in this note. The selection procedures for each analysis are detailed in Refs. [13] through [24], and are briefly described below.

II. SUMMARY OF INCLUDED ANALYSES

For the $WH \to \ell\nu b\bar{b}$ analyses, events are analyzed in two and three jet sub-channels separately, and in each of these samples the events are grouped into various charged lepton and b-tag categories. Events are broken into separate analysis categories based on the quality of the identified lepton. Separate categories are used for events with a high quality central muon or electron candidate, an isolated track or identified loose muon in the extended muon coverage, a forward electron candidate, and a loose central electron or isolated track candidate. The latter two lepton categories, which provide some acceptance for lower quality electrons and single prong tau decays, are used only in the case of two-jet events. Within the lepton categories there are five b-tagging categories considered for two-jet events: two tight b-tags (TT), one tight b-tag and one loose b-tag (TL), a single tight b-tag (Tx), two loose b-tags (LL), and a single loose b-tag definitions are taken for the first time from a neural network tagging algorithm (HOBIT) [9] based on sets of kinematic variables sensitive to displaced decay vertices and tracks within jets with large transverse impact parameters relative to the hard-scatter vertices. Using an operating point which gives an equivalent rate of false tags, the new algorithm improves upon previous b-tagging efficiencies by $\sim 20\%$. A Bayesian neural network discriminant is trained at each Higgs boson mass within the test range for each of the specific categories (defined by lepton type, b-tagging type, and number of jets) to separate signal from backgrounds.

For the $ZH \to \nu \bar{\nu}bb$ analyses, the selection is similar to the WH selection, except all events with isolated charged leptons are rejected and stronger multijet background suppression techniques are applied. A track-based missing

transverse momentum calculation is used as an additional discriminant against false calorimeter E_T . We utilize multi-variate techniques, an artificial neural network, to further discriminate against the multijet background before b-tagging. There is a sizable fraction of the $WH \to \ell \nu b\bar{b}$ signal in which the lepton is undetected that is selected in the $ZH \to \nu \bar{\nu} b\bar{b}$ samples, so these analyses are also referred to as $VH \to E_T b\bar{b}$. The events are divided into three non-overlapping categories of b-tagged events (SS, SJ and 1S). These categories are based on two older b-tagging algorithms, an algorithm for reconstructing displaced, secondary vertices of b-quark decays (S) and an algorithm for assigning a likelihood for tracks within a jet to have originated from a displaced vertex (J). The final analysis uses a second layer of neural network discriminants for separating signal from backgrounds.

The $ZH \to \ell^+\ell^-b\bar{b}$ analyses require two isolated charged leptons and at least two jets. The analysis incorporates the new neural network b-tagging algorithm and divides events into four out of the five WH tagging categories (TT, TL, Tx, and LL). Events with 2 or 3 jets are also now separated into independent analysis channels. We use neural networks to select loose electron and muon candidates for reconstructing Z boson candidates. Jet energies are corrected for the E_T resulting from jet mis-measurement using a neural network approach. We utilize a multi-layer discriminant based on neural networks where separate discriminant functions are used to define four separate regions of the final discriminant function.

We separate the $H \to W^+W^-$ events into five non-overlapping samples, split into "high s/b" and "low s/b" categories defined by charged lepton types and the number of reconstructed jets: 0, 1, or 2+ jets. The sample with two or more jets is not split into low s/b and high s/b lepton categories due to the smaller statistics in this channel. A sixth channel is the low dilepton mass $(m_{\ell^+\ell^-})$ channel, which accepts events with $m_{\ell^+\ell^-} < 16 \text{ GeV}/c^2$. We further improve the analysis of the low dilepton mass channel by reducing the ΔR cut applied to dilepton pairs down to 0.1, which increases Higgs signal acceptance in this channel $\sim 10\%$.

The division of events into categories based on the number of reconstructed jets allows the analysis discriminants to separate differing contributions of signal and background processes more effectively. The signal production mechanisms considered are $gg \to H \to W^+W^-$, $WH + ZH \to jjW^+W^-$, and vector-boson fusion. The relative fractions of the contributions from each of the three signal processes and background processes, notably W^+W^- production and $t\bar{t}$ production, are very different in the different jet categories. Dividing our data into these categories provides more statistical discrimination, but introduces the need to evaluate the systematic uncertainties carefully in each jet category. A discussion of these uncertainties is found in Section III.

The $H \to W^+W^-$ analyses use neural-network outputs, including likelihoods constructed from calculated matrixelement probabilities as additional inputs for the 0-jet bin.

We include a separate analysis of events with same-sign leptons to incorporate additional potential signal from associated production events in which the two leptons (one from the associated vector boson and one from a W boson produced in the Higgs boson decay) have the same charge. We additionally incorporate three tri-lepton channels to include additional associated production contributions where leptons result from the associated W boson and the two W bosons produced in the Higgs boson decay or where an associated Z boson decays into a pair of leptons and a third lepton is produced in the decay of either of the W bosons resulting from the Higgs decay. In the latter case, the sample is separated into one jet and two or more jet sub-channels to take full advantage of the fact that the Higgs boson candidate mass can be reconstructed from the invariant mass of the two jets, the lepton, and the missing transverse energy. For the first time, we include a new tri-lepton channel focusing on WH production in which one of the three leptons is reconstructed as a hadronic tau.

We include a search for $H \to ZZ$ in events with four charged leptons. In addition to the simple four-lepton invariant mass discriminant used previously for separating potential Higgs boson signal events from the non-resonant ZZ background, the E_T in these events is now used as a second discriminating variable to better identify four lepton signal contributions from $ZH \to ZWW$ and $ZH \to Z\tau\tau$ production. We have also updated its opposite-sign channels in which one of the two lepton candidates is a hadronic tau. Events are separated into e- τ and μ - τ channels. The final discriminants are obtained from boosted decision trees that incorporate both hadronic tau identification and kinematic event variables as inputs.

We incorporate an updated all-hadronic analysis based on the older b-tagging algorithms, which results in two sub-channels (SS and SJ). Both WH/ZH and VBF production contribute to the $jjb\bar{b}$ final state. Events with either four or five reconstructed jets are selected, and at least two must be b-tagged. The large QCD multijet backgrounds are modeled from the data by applying a measured mistag probability to the non b-tagged jets in events containing a single b-tag. Neural network discriminants based on kinematic event variables including those designed to separate

quark and gluon jets are used to obtain the final limits.

We include an updated, generic analysis searching for Higgs bosons decaying to tau lepton pairs incorporating contributions from direct $gg \to H$ production, associated WH or ZH production, and vector boson production. We also include an analysis of events that contain one or more reconstructed leptons ($\ell = e$ or μ) in addition to a tau lepton pair focusing on associated production where $H \to \tau\tau$ and additional leptons are produced in the decay of the W or Z boson. For these searches multiple Support Vector Machine (SVM) [25] classifiers are obtained using separate trainings for the signal against each of the primary backgrounds. In the generic search, events with either one or two jets are separated into two independent analysis channels. The final discriminant for setting limits is obtained using the minimum score of four SVM classifiers obtained from trainings against the primary backgrounds ($Z \to \tau\tau$, $t\bar{t}$, multi-jet, and W+jet production). In the extended analysis events are separated into five separate analysis channels ($\ell\ell\ell$, $e\mu\tau_{\rm had}$, $\ell\ell\tau_{\rm had}$, $\ell\tau_{\rm had}$, and $\ell\ell\ell\ell$). The four lepton category includes $\tau_{\rm had}$ candidates. The final discriminants are likelihoods based on outputs obtained from independent SVM trainings against each of the primary backgrounds (Z+jets, $t\bar{t}$, and dibosons). These channels are included in the combination only for lower Higgs masses to avoid overlap with other search channels.

Also included in the combination is an analysis that searches for the decay $H \to \gamma \gamma$. This analysis looks for a signal peak in the diphoton invariant mass spectrum above the smooth background originating from standard QCD multijet production. Events are now separated into four independent analysis channels based on the photon candidates contained within the event: two central candidates (CC), one central and one plug candidate (CP), one central and one central conversion candidate (PC-Conv).

We incorporate three non-overlapping sets of analysis channels searching for the process $t\bar{t}H\to t\bar{t}b\bar{b}$. One set of channels selects events with a reconstructed charged lepton, large missing transverse energy, and four or five reconstructed jets. These events are further sub-divided into five b-tagging categories based on the older tagging algorithms (three tight b-tags (SSS), two tight and one loose b-tags (SSJ), one tight and two loose b-tags (SJJ), two tight b-tags (SS), and one tight and one loose b-tags (SJ)). Neural network discriminants trained at each mass point are used to set limits. A second set of channels selects events with no reconstructed lepton. These events are separated into two categories, one containing events with large missing transverse energy and five to nine reconstructed jets and another containing events with low missing transverse energy and seven to ten reconstructed jets. Events in these two channels are required to have a minimum of two b-tagged jets. Events with three or more b-tags are analyzed in separate channels from those with exactly two tags. Two stages of neural network discriminants are used (the first to help reject large multijet backgrounds and the second to separate potential $t\bar{t}H$ signal events from $t\bar{t}$ background events).

Events with false charged leptons or E_T from QCD multijet backgrounds are typically measured in independent data samples using several different methods. Backgrounds from SM processes with electroweak gauge bosons or top quarks were generated using PYTHIA, ALPGEN [63], MC@NLO [64], and HERWIG [65] programs. These background processes were normalized using either experimental data or next-to-leading order calculations (including MCFM [67] for the W+ heavy flavor process).

Table II summarizes the integrated luminosities, the Higgs boson mass ranges over which the searches are performed, and references to further details for each analysis.

III. SIGNAL PREDICTIONS

We normalize our Higgs boson signal predictions to the most recent high-order calculations available. The $gg \to H$ production cross section we use is calculated at next-to-next-to leading order (NNLO) in QCD with a next-to-next-to leading log (NNLL) resummation of soft gluons; the calculation also includes two-loop electroweak effects and handling of the running b quark mass [29, 30]. The numerical values in Table I are updates [31] of these predictions with m_t set to 173.1 GeV/ c^2 [32], and an exact treatment of the massive top and bottom loop corrections up to next-to-leading-order (NLO) + next-to-leading-log (NLL) accuracy. The factorization and renormalization scale choice for this calculation is $\mu_F = \mu_R = m_H$. These calculations are refinements of the earlier NNLO calculations of the $gg \to H$ production cross section [35–37]. Electroweak corrections were computed in Refs. [38, 39]. Soft gluon resummation was introduced in the prediction of the $gg \to H$ production cross section in Ref. [40]. The $gg \to H$ production cross section depends strongly on the gluon parton density function, and the accompanying value of $\alpha_s(q^2)$. The cross

sections used here are calculated with the MSTW 2008 NNLO PDF set [41], as recommended by the PDF4LHC working group [42]. The inclusive Higgs boson production cross sections are listed in Table I.

For analyses that consider inclusive $gg \to H$ production but do not split it into separate channels based on the number of reconstructed jets, we use the inclusive uncertainties from the simultaneous variation of the factorization and renormalization scale up and down by a factor of two. We use the prescription of the PDF4LHC working group for evaluating PDF uncertainties on the inclusive production cross section. QCD scale uncertainties that affect the cross section via their impacts on the PDFs are included as a correlated part of the total scale uncertainty. The remainder of the PDF uncertainty is treated as uncorrelated with the QCD scale uncertainty.

For analyses seeking $gg \to H$ production that divide events into categories based on the number of reconstructed jets, we employ a new approach for evaluating the impacts of the scale uncertainties. Following the recommendations of Ref. [33], we treat the QCD scale uncertainties obtained from the NNLL inclusive [29, 30], NLO one or more jets [26], and NLO two or more jets [34] cross section calculations as uncorrelated with one another. We then obtain QCD scale uncertainties for the exclusive $gg \to H+0$ jet, 1 jet, and 2 or more jet categories by propagating the uncertainties on the inclusive cross section predictions through the subtractions needed to predict the exclusive rates. For example, the H+0 jet cross section is obtained by subtracting the NLO H+1 or more jet cross section from the inclusive NNLL+NNLO cross section. We now assign three separate, uncorrelated scale uncertainties which lead to correlated and anticorrelated uncertainty contributions between exclusive jet categories. The procedure in Ref. [26] is used to determine PDF model uncertainties. These are obtained separately for each jet bin.

The scale choice affects the p_T spectrum of the Higgs boson when produced in gluon-gluon fusion, and this effect changes the acceptance of the selection requirements and also the shapes of the distributions of the final discriminants. The effect of the acceptance change is included in the calculations of Ref. [26] and Ref. [34], as the experimental requirements are simulated in these calculations. The effects on the final discriminant shapes are obtained by reweighting the p_T spectrum of the Higgs boson production in our Monte Carlo simulation to higher-order calculations. The Monte Carlo signal simulation used by CDF and D0 is provided by the LO generator PYTHIA [56] which includes a parton shower and fragmentation and hadronization models. We reweight the Higgs boson p_T spectra in our PYTHIA Monte Carlo samples to that predicted by HQT [27] when making predictions of differential distributions of $gg \to H$ signal events. To evaluate the impact of the scale uncertainty on our differential spectra, we use the RESBOS [28] generator, and apply the scale-dependent differences in the Higgs boson p_T spectrum to the HQT prediction, and propagate these to our final discriminants as a systematic uncertainty on the shape, which is included in the calculation of the limits.

We include all significant Higgs production modes in the high-mass search. Besides gluon-gluon fusion through virtual quark loops (ggH), we include Higgs boson production in association with a W or Z vector boson (VH), and vector boson fusion (VBF). For the low-mass searches, we target the WH, ZH, VBF, and $t\bar{t}H$ [49] production modes with specific searches, including also those signal components not specifically targeted but which fall in the acceptance nonetheless. Our WH and ZH cross sections are from Ref. [50]. This calculation starts with the NLO calculation of V2HV [51] and includes NNLO QCD contributions [52], as well as one-loop electroweak corrections [53]. We use the VBF cross section computed at NNLO in QCD in Ref. [54]. Electroweak corrections to the VBF production cross section are computed with the HAWK program [55], and are small and negative (2-3%) in the Higgs boson mass range considered here. We include these corrections in the VBF cross sections used for this result. The $t\bar{t}H$ production cross sections we use are from Ref. [49].

In order to predict the kinematic distributions of Higgs boson signal events, we use the PYTHIA [56] Monte Carlo program, with CTEQ5L and CTEQ6L [57] leading-order (LO) parton distribution functions. The Higgs boson decay branching ratio predictions used for this result are those of Ref. [58]. In this calculation, the partial decay widths for all Higgs boson decays except to pairs of W and Z bosons are computed with HDECAY [59], and the W and Z pair decay widths are computed with PROPHECY4F [60]. The relevant decay branching ratios are listed in Table I. The uncertainties on the predicted branching ratios from uncertainties in m_b , m_c , and α_s and missing higher-order effects are presented in Ref. [61, 62].

Table II summarizes the integrated luminosities, the Higgs boson mass ranges over which the searches are performed, and references to further details for each analysis.

TABLE I: The production cross sections and decay branching fractions for the SM Higgs boson assumed for the combination.

m_H	$\sigma_{gg \to H}$	σ_{WH}	σ_{ZH}	σ_{VBF}	$\sigma_{t\bar{t}H}$	$B(H \to b\bar{b})$	$B(H \to c\bar{c})$	$B(H \to \tau^+ \tau^-)$	$B(H \to W^+W^-)$	$B(H \to ZZ)$	$B(H \to \gamma \gamma)$
(GeV/c^2)	(fb)	(fb)	(fb)	(fb)	(fb)	(%)	(%)	(%)	(%)	(%)	(%)
100	1821.8	281.1	162.7	97.3	8.000	79.1	3.68	8.36	1.11	0.113	0.159
105	1584.7	238.7	139.5	89.8	7.062	77.3	3.59	8.25	2.43	0.215	0.178
110	1385.0	203.7	120.2	82.8	6.233	74.5	3.46	8.03	4.82	0.439	0.197
115	1215.9	174.5	103.9	76.5	5.502	70.5	3.27	7.65	8.67	0.873	0.213
120	1072.3	150.1	90.2	70.7	4.857	64.9	3.01	7.11	14.3	1.60	0.225
125	949.3	129.5	78.5	65.3	4.279	57.8	2.68	6.37	21.6	2.67	0.230
130	842.9	112.0	68.5	60.5	3.769	49.4	2.29	5.49	30.5	4.02	0.226
135	750.8	97.2	60.0	56.0	3.320	40.4	1.87	4.52	40.3	5.51	0.214
140	670.6	84.6	52.7	51.9	2.925	31.4	1.46	3.54	50.4	6.92	0.194
145	600.6	73.7	46.3	48.0	2.593	23.1	1.07	2.62	60.3	7.96	0.168
150	539.1	64.4	40.8	44.5	2.298	15.7	0.725	1.79	69.9	8.28	0.137
155	484.0	56.2	35.9	41.3	2.037	9.18	0.425	1.06	79.6	7.36	0.100
160	432.3	48.5	31.4	38.2	1.806	3.44	0.159	0.397	90.9	4.16	0.0533
165	383.7	43.6	28.4	36.0	1.607	1.19	0.0549	0.138	96.0	2.22	0.0230
170	344.0	38.5	25.3	33.4	1.430	0.787	0.0364	0.0920	96.5	2.36	0.0158
175	309.7	34.0	22.5	31.0	1.272	0.612	0.0283	0.0719	95.8	3.23	0.0123
180	279.2	30.1	20.0	28.7	1.132	0.497	0.0230	0.0587	93.2	6.02	0.0102
185	252.1	26.9	17.9	26.9	1.004	0.385	0.0178	0.0457	84.4	15.0	0.00809
190	228.0	24.0	16.1	25.1	0.890	0.315	0.0146	0.0376	78.6	20.9	0.00674
195	207.2	21.4	14.4	23.3	0.789	0.270	0.0125	0.0324	75.7	23.9	0.00589
200	189.1	19.1	13.0	21.7	0.700	0.238	0.0110	0.0287	74.1	25.6	0.00526

TABLE II: Luminosity, explored mass range and references for the different processes and final states ($\ell = e$ or μ) for the CDF analyses. The generic labels "2×", "3×", and "4×" refer to separations based on lepton categories.

Channel	Luminosity (fb^{-1})	m_H range (GeV/c^2)	Reference
$WH \rightarrow \ell\nu b\bar{b}$ 2-jet channels $4\times (TT,TL,Tx,LL,Lx)$	9.45	100-150	[13]
$WH \to \ell \nu b \bar{b}$ 3-jet channels $3 \times (TT, TL)$	9.45	100-150	[13]
$ZH \to \nu \bar{\nu} b \bar{b}$ (SS,SJ,1S)	9.45	100-150	[14]
$ZH \to \ell^+\ell^-b\bar{b}$ 2-jet channels $2\times (TT,TL,Tx,LL)$	9.45	100-150	[15]
$ZH \to \ell^+\ell^-b\bar{b}$ 3-jet channels $2\times (TT,TL,Tx,LL)$	9.45	100-150	[15]
$H \to W^+W^-$ 2×(0 jets,1 jet)+(2 or more jets)+(low- $m_{\ell\ell}$)	9.7	110-200	[16]
$H o W^+W^- (e ext{-} au_{ m had}) + (\mu ext{-} au_{ m had})$	9.7	130-200	[17]
$WH \to WW^+W^-$ (same-sign leptons)+(tri-leptons)	9.7	110-200	[16]
$WH \to WW^+W^-$ tri-leptons with 1 $\tau_{\rm had}$	9.7	110-200	[17]
$ZH \to ZW^+W^-$ (tri-leptons with 1 jet)+(tri-leptons with 2 or more jets)	9.7	130-200	[16]
$H \to ZZ$ four leptons	9.7	120-200	[18]
$H + X \rightarrow \tau^+ \tau^-$ (1 jet)+(2 jets)	8.3	100-150	[19]
$WH ightarrow \ell u au^+ au^- / ZH ightarrow \ell^+ \ell^- au^+ au^- \qquad \ell^- au_{ m had} ^- au_{ m had}$	6.2	100-150	[20]
$WH o \ell u au^+ au^- / ZH o \ell^+ \ell^- au^+ au^- \qquad (\ell ext{-}\ell ext{-} au_{ m had}) + (e ext{-}\mu ext{-} au_{ m had})$	6.2	100-125	[20]
$WH ightarrow \ell u au^+ au^- / ZH ightarrow \ell^+ \ell^- au^+ au^- \qquad \ell ext{-}\ell ext{-}\ell$	6.2	100-105	[20]
$ZH \to \ell^+\ell^-\tau^+\tau^-$ four leptons including $\tau_{\rm had}$ candidates	6.2	100-115	[20]
$WH + ZH \rightarrow jjb\bar{b}$ (SS,SJ)	9.45	100-150	[21]
$H \to \gamma \gamma$ (CC,CP,CC-Conv,PC-Conv)	10.0	100-150	[22]
$t\bar{t}H \to WWb\bar{b}b\bar{b}$ (lepton) (4jet,5jet, \geq 6jet) \times (SSS,SSJ,SJJ,SS,SJ)	9.45	100 - 145	[23]
$t\bar{t}H \to WWb\bar{b}b\bar{b}$ (no lepton) (low met,high met)×(2 tags,3 or more tags)	5.7	100-150	[24]

IV. DISTRIBUTIONS OF CANDIDATES

All analyses provide binned histograms of the final discriminant variables for the signal and background predictions, itemized separately for each source, and the observed data. The number of channels combined is large, and the number of bins in each channel is large. Therefore, the task of assembling histograms and checking whether the expected and observed limits are consistent with the input predictions and observed data is difficult. We therefore provide histograms that aggregate all channels' signal, background, and data together. In order to preserve most of the sensitivity gain that is achieved by the analyses by binning the data instead of collecting them all together and counting, we aggregate the data and predictions in narrow bins of signal-to-background ratio, s/b. Data with similar s/b may be added together with no loss in sensitivity, assuming similar systematic errors on the predictions. The aggregate histograms do not show the effects of systematic uncertainties, but instead compare the data with the central predictions supplied by each analysis.

The range of s/b is quite large in each analysis, and so $\log_{10}(s/b)$ is chosen as the plotting variable. Plots of the distributions of $\log_{10}(s/b)$ are shown for Higgs boson masses of 115, 120, 125, 135, 165 and 200 GeV/ c^2 in Figure 1. These distributions can be integrated from the high-s/b side downwards, showing the sums of signal, background, and data for the most pure portions of the selection of all channels added together. These integrals can be seen in Figure 2. The most significant candidates are found in the bins with the highest s/b; an excess in these bins relative to the background prediction drives the Higgs boson cross section limit upwards, while a deficit drives it downwards. The lower-s/b bins show that the modeling of the rates and kinematic distributions of the backgrounds is very good. The integrated plots show a slight excess of events in the highest-s/b bins for the analyses searching for a Higgs boson mass of 115 GeV/ c^2 , and a slight deficit of events in the highest-s/b bins for the analyses searching for a Higgs boson of mass $165 \text{ GeV}/c^2$.

We also show the distributions of the data after subtracting the expected background, and compare that with the expected signal yield for a Standard Model Higgs boson, after collecting all bins in all channels sorted by s/b. These

background-subtracted distributions are shown in Figure 3. These graphs also show the remaining uncertainty on the background prediction after fitting the background model to the data within the systematic uncertainties on the rates and shapes in each contributing channel's templates.

V. COMBINING CHANNELS

We combine the results of the searches using a Bayesian technique, described below, which relies on distributions in the final discriminants, and not just on their single integrated values. Systematic uncertainties enter on the predicted number of signal and background events as well as on the distribution of the discriminants in each analysis ("shape uncertainties"). Both methods use likelihood calculations based on Poisson probabilities.

A. Statistical Method

We choose to use a Bayesian statistical method [10], with a flat prior assumed for the total number of selected Higgs events. For a given Higgs boson mass, the combined likelihood is a product of likelihoods for the individual channels, each of which is a product over histogram bins:

$$\mathcal{L}(R, \vec{s}, \vec{b} | \vec{n}, \vec{\theta}) \times \pi(\vec{\theta}) = \prod_{i=1}^{N_C} \prod_{j=1}^{N_b} \mu_{ij}^{n_{ij}} e^{-\mu_{ij}} / n_{ij}! \times \prod_{k=1}^{n_{np}} e^{-\theta_k^2/2}$$
(1)

where the first product is over the number of channels (N_C) , and the second product is over N_b histogram bins containing n_{ij} events, binned in ranges of the final discriminants used for individual analyses, such as the dijet mass, neural-network outputs, or matrix-element likelihoods. The parameters that contribute to the expected bin contents are $\mu_{ij} = R \times s_{ij}(\vec{\theta}) + b_{ij}(\vec{\theta})$ for the channel i and the histogram bin j, where s_{ij} and b_{ij} represent the expected background and signal in the bin, and R is a scaling factor applied to the signal to test the sensitivity level of the experiment. Truncated Gaussian priors are used for each of the nuisance parameters θ_k , which define the sensitivity of the predicted signal and background estimates to systematic uncertainties. These can take the form of uncertainties on overall rates, as well as the shapes of the distributions used for combination. These systematic uncertainties can be far larger than the expected SM Higgs boson signal, and are therefore important in the calculation of limits. The truncation is applied so that no prediction of any signal or background in any bin is negative. The posterior density function is then integrated over all parameters (including correlations) except for R, and a 95% credibility level upper limit on R is estimated by calculating the value of R that corresponds to 95% of the area of the resulting distribution.

B. Systematic Uncertainties

Systematic uncertainties differ between analyses, and they affect the rates and shapes of the predicted signal and background in correlated ways. The combined results incorporate the sensitivity of predictions to values of nuisance parameters, and include correlations between rates and shapes, between signals and backgrounds, and between channels. More on these issues can be found in the individual analysis notes [?] through [24]. Here we consider only the largest contributions and correlations between and within the two experiments.

1. Correlated Systematics Between Channels

The uncertainty on the measurement of the integrated luminosity is 6%. Of this value, 4% arises from the uncertainty on the inelastic $p\bar{p}$ scattering cross section. All predictions of signals and backgrounds that rely on theoretical cross section predictions that are scaled by the integrated luminosity share this common source of systematic uncertainty.

Most channels presented here also share the assumed values and uncertainties on the production cross sections for top-quark processes ($t\bar{t}$ and single top) and for electroweak processes (WW, WZ, and ZZ). In order to provide a consistent combination, the values of these cross sections assumed in each analysis are brought into agreement. We use $\sigma_{t\bar{t}} = 7.04^{+0.24}_{-0.36}$ (scale) ± 0.14 (PDF) ± 0.30 (mass), following the calculation of Moch and Uwer [70], assuming a top quark mass $m_t = 173.0 \pm 1.2$ GeV/ c^2 [71], and using the MSTW2008nnlo PDF set [41]. Other calculations of $\sigma_{t\bar{t}}$ are similar [72].

For single top, we use the NLL t-channel calculation of Kidonakis [73], which has been updated using the MSTW2008nnlo PDF set [41] [74]. For the s-channel process we use [75], again based on the MSTW2008nnlo PDF set. Both of the cross section values below are the sum of the single t and single t cross sections, and both assume $m_t = 173 \pm 1.2$ GeV.

$$\sigma_{t-\text{chan}} = 2.10 \pm 0.027 \text{ (scale)} \pm 0.18 \text{ (PDF)} \pm 0.045 \text{ (mass) pb.}$$
 (2)

$$\sigma_{s-\text{chan}} = 1.046 \pm 0.006 \text{ (scale)} \pm 0.059 \text{ (PDF)} \pm 0.030 \text{ (mass) pb.}$$
 (3)

Other calculations of $\sigma_{\text{SingleTop}}$ are similar for our purposes [76].

MCFM [67] has been used to compute the NLO cross sections for WW, WZ, and ZZ production [77]. Using a scale choice $\mu_0 = M_V^2 + p_T^2(V)$ and the MSTW2008 PDF set [41], the cross section for inclusive W^+W^- production is

$$\sigma_{W^+W^-} = 11.34^{+0.56}_{-0.49} \text{ (scale)} ^{+0.35}_{-0.28} \text{ (PDF) pb}$$
 (4)

and the cross section for inclusive $W^{\pm}Z$ production is

$$\sigma_{W^{\pm}Z} = 3.22^{+0.20}_{-0.17} \text{ (scale)} ^{+0.11}_{-0.08} \text{ (PDF) pb}$$
 (5)

For the Z, leptonic decays are used in the definition, with both γ and Z exchange. The cross section quoted above involves the requirement $75 \le m_{\ell^+\ell^-} \le 105$ GeV for the leptons from the neutral current exchange. The same dilepton invariant mass requirement is applied to both sets of leptons in determining the ZZ cross section which is

$$\sigma_{ZZ} = 1.20^{+0.05}_{-0.04} \text{ (scale)} ^{+0.04}_{-0.03} \text{ (PDF) pb}$$
 (6)

For the diboson cross section calculations, $|\eta_{\ell}| < 5$ for all calculations. Loosening this requirement to include all leptons leads to $\sim +0.4\%$ change in the predictions. Lowering the factorization and renormalization scales by a factor of two increases the cross section, and raising the scales by a factor of two decreases the cross section. The PDF uncertainty has the same fractional impact on the predicted cross section independent of the scale choice. All PDF uncertainties are computed as the quadrature sum of the twenty 68% C.L. eigenvectors provided with MSTW2008 (MSTW2008nlo68cl).

In many analyses, the dominant background yields are calibrated with data control samples. Since the methods of measuring the multijet ("QCD") backgrounds differ between analyses, there is no correlation assumed between these rates. Similarly, the large uncertainties on the background rates for W+heavy flavor (HF) and Z+heavy flavor are considered at this time to be uncorrelated, as the several analyses that are sensitive to this parameter employ different techniques to estimate its central value, which is obscured by effects of acceptance and efficiency being different between the analyses. The calibrations of fake leptons, unvetoed $\gamma \to e^+e^-$ conversions, b-tag efficiencies and mistag rates are performed by each collaboration using independent data samples and methods, and are therefore also treated as uncorrelated.

2. Systematic Uncertainties for Each Channel

The dominant systematic uncertainties for the analyses combined in this note are shown in the Appendix in Tables IV and V for the $WH \to \ell\nu b\bar{b}$ channels, in Table VI for the $WH, ZH \to E/D\bar{b}$ channels, in Tables VII and VIII for the $ZH \to \ell^+\ell^-b\bar{b}$ channels, in Tables IX, X, and XI for the $H \to W^+W^- \to \ell'^\pm\nu\ell'^\mp\nu$ channels, in Table XII for the

 $WH \to WWW \to \ell'^\pm \ell'^\pm$ and $WH \to WWW \to \ell^\pm \ell'^\pm \ell''^\mp$ channels, in Table XIII for the $ZH \to ZWW \to \ell^\pm \ell'^\pm$ channels, In Table XIV for the $H \to 4\ell$ channel, in Tables XV, XVI, and XVII for the $t\bar{t}H \to W^+bW^-\bar{b}b\bar{b}$ channels, in Table XVIII for the $H \to \tau^+\tau^-$ channels, in Table XIX for the $WH \to \ell\nu\tau^+\tau^-$ and $ZH \to \ell^+\ell^-\tau^+\tau^-$ channels, in Table XX for the WH/ZH and VBF $\to jjb\bar{b}$ channels, and in Table XXI for the $H \to \gamma\gamma$ channel. Each source induces a correlated uncertainty across all CDF channels' signal and background contributions which are sensitive to that source. For $H \to b\bar{b}$, the largest uncertainties on signal arise from measured b-tagging efficiencies, jet energy scale, and other Monte Carlo modeling. Shape dependencies of templates on jet energy scale, b-tagging, and gluon radiation ("ISR" and "FSR") are taken into account for some analyses (see tables). For $H \to W^+W^-$, the largest uncertainties on signal acceptance originate from Monte Carlo modeling. Uncertainties on background event rates vary significantly for the different processes. The backgrounds with the largest systematic uncertainties are in general quite small. Such uncertainties are constrained by fits to the nuisance parameters, and they do not affect the result significantly. Because the largest background contributions are measured using data, these uncertainties are treated as uncorrelated for the $H \to b\bar{b}$ channels. The differences in the resulting limits when treating the remaining uncertainties as either correlated or uncorrelated, is less than 5%.

VI. COMBINED RESULTS

Using the combination procedure outlined in Section III, we extract limits on SM Higgs boson production $\sigma \times B(H \to X)$ in $p\bar{p}$ collisions at $\sqrt{s} = 1.96$ TeV for $100 \le m_H \le 200$ GeV/ c^2 . To facilitate comparisons with the standard model and to accommodate analyses with different degrees of sensitivity, we present our results in terms of the ratio of obtained limits to the SM Higgs boson production cross section, as a function of Higgs boson mass, for test masses for which we have performed dedicated searches in different channels. A value of the combined limit ratio which is less than or equal to one indicates that that particular Higgs boson mass is excluded at the 95% C.L.

The combinations of CDF's search results yield ratios of 95% C.L. observed (expected) limits to the SM cross section of 2.25 (1.16) for $m_H = 115 \text{ GeV}/c^2$, and 0.41 (0.67) for $m_H = 165 \text{ GeV}/c^2$.

The ratios of the 95% C.L. expected and observed limit to the SM cross section are shown in Figure 4 for the combined CDF analyses. The observed and median expected ratios are listed for the tested Higgs boson masses in Table III. A broad excess in the observed limit is evident between 100 and 140 GeV/c^2 , reaching beyond 2σ at 120 GeV/c^2 . An excess is also seen above 2 σ at 190 GeV/c^2 .

We further break down this combination by Higgs decay mode in order to demonstrate the nature of this excess. Figures 5, 6, 7 show the ratios of the 95% C.L. expected and observed limit to the SM cross section separated by channel according to the Higgs decays of $H \to b\bar{b}$, $H \to W^+W^-$, and $H \to \gamma\gamma$. The $H \to b\bar{b}$ channels provide the largest excess in the observed limits above the expected, reaching greater than 2σ from 115 to 145 GeV/ c^2 . The expected limit is $1.2\times SM$ at 115 GeV/ c^2 , and $6.0\times SM$ at 145 GeV/ c^2 . The excess is more consistent with a SM Higgs signal when the expected limit is close to $1\times SM$. The $H\to W^+W^-$ channels show a greater than 2σ fluctuation above 194 GeV/ c^2 , where the sensitivity is between 2 and $3\times SM$. The $H\to \gamma\gamma$ channels do not reach an expected sensitivity below $10\times SM$ across the full mass range and demonstrate no fluctuations greater than 2σ .

Given there is an excess, we perform a best fit of the signal cross section to the observed data allowing nuisance parameters to vary. The results are shown in Figure 8 for a simultaneous fit to all channels also for just the associated production $H \to b\bar{b}$ channels. The best fit of all channels shows the most significant signal cross section peaked at 120 GeV/c^2 , and rising again at 190 GeV/c^2 . The best fit of the $H \to b\bar{b}$ channels shows a steadily rising signal stength from 90 to 150 GeV/c^2 . The $H \to b\bar{b}$ behavior is what would be expected for a signal below 130 GeV/c^2 . Given that the mass resolution for these channels is broad and the expected cross-section times branching ratio is decreasing steadily as a function of mass, a 120 GeV/c^2 signal with standard model strength would appear to be larger than that predicted bt the standard model when searched for at higher mass. While the $H \to b\bar{b}$ channels are sensitive to a Higgs boson in the mass range of 115 to 130 GeV/c^2 , the sensitivity worsens to greater than $10 \times \text{SM}$ by about $140 \text{ GeV}/c^2$ due to the falling cross-sections and branching ratio, so small upward fluctations in the background can yield large estimates of signal strength. When all channels are taken into account, the high signal cross section from

the $H \to b\bar{b}$ channels above 120 GeV/ c^2 is mediated by the $H \to W^+W^-$ channels which gain in sensitivity as a function of mass, until they completely dominate the combined sensitivity at around 140 GeV/ c^2 . At 190 GeV/ c^2 , the combined fit shows a large excess in signal. Above 185 GeV/ c^2 , however, is where the CDF sensitivity is the poorest in the 100 - 200 GeV/ c^2 mass range, such that background fluctuations yield large signal cross section fits.

We also perform a test to determine how often the background model, without a Higgs boson signal, can generate an excess as large as the one seen in the observed data. To do this we generate a large set of pseudo-experiments, in which the background is allowed to fluctuate according to statistical and systematic variations, and from these build a distribution of signal cross section fits. A background p-value can be determined from this distribution based on how likely the background is to produce a given fitted signal cross section or larger value. Figure 9 shows the p-value, and its associated significance in units of standard deviation, for all channels, and for $H \to b\bar{b}$ channels separately. The dashed line represents how often the background fluctuates to a produce a standard model signal cross section or larger. The uncertainty bands indicate 1 and 2 standard deviations from the dashed line. The minimum p-value for all search channels corresponds to a 2.6 σ level local significance at 120 GeV/ c^2 . The minimum p-value for the $H \to b\bar{b}$ channels corresponds to a 2.9 σ level local significance at 135 GeV/ c^2 .

These probabilities do not include the look-elsewhere effect (LEE), and are thus local p-values, corresponding to searches for each value of m_H separately. The LEE accounts for the probability of observing an upwards fluctuation of the background at any of the tested values of m_H in our region of interest, at least as significant as the one observed at the value of m_H with the most significant local excess. A simple and correct method of calculating the LEE, and thus the global significance of the excess, is to simulate many possible experimental outcomes assuming the absence of a signal, and for each one, compute the LLR curve and find the deviation with the smallest background-only-hypothesis p-value. Using this minimum p-value as a test statistic, another p-value is then computed, which is the probability of observing that minimum p-value or less. This method is difficult to pursue in the Tevatron Higgs boson searches due to the fact that in most search analysis, a distinct multivariate analysis (MVA) discriminant function is trained for each value of m_H that is tested. This step is an important optimization, because the kinematic distributions and branching ratios are functions of m_H , but it introduces the difficulty of running the same set of simulated events separately through many MVA functions in order to compute the LEE with the simple method. The use of a separate MVA function at each m_H also introduces additional point-to-point randomness as individual events are reclassified from bins with lower s/b to higher and vice versa. Even though the discriminants are nearly optimal and are thus highly similar from one m_H value to the next, small variations are amplified by the discrete nature of the data which are processed through these networks. One may see this in the variations in the observed limits, LLR values and p-values from one mass point to the next which show more rapid variation than can be explained by mass resolution alone.

Gross and Vitells [78] provide a technique that extrapolates from a smaller sample of background-only Monte Carlo simulations fully propagated through the MVA's. We lack the ability to perform this propagation through all of our channels, as we rely on exchanged histograms of distributions of selected events. We therefore estimate the LEE effect in a simplified manner. In the mass range $100-150~GeV/c^2$, where the low-mass $H \to b\bar{b}$ searches dominate, the reconstructed mass resolution is approximately 10-15%, or about $15~GeV/c^2$. However, the multivariate discriminants used in the searches are trained to distinguish signal from background, not measure its mass, and have worse Higgs mass resolution than the dijet mass distribution itself. We therefore estimate a LEE factor of ~ 2 for the low-mass region. The $H \to \gamma \gamma$ searches have a much better mass resolution, of order 3%, but their contribution to the final LLR is small due to the very much smaller s/b in those searches. They introduce more rapid oscillations of LLR as a function of m_H , but the magnitude of these oscillations is much smaller than those induced by the $H \to b\bar{b}$ searches. The $H \to \tau^+\tau^-$ searches have both less reconstructed mass resolution and lower s/b than the $H \to b\bar{b}$ searches and similarly do not play much of a role in the estimation of LEE.

For the high-mass searches, the $H \to W^+W^-$ searches dominate the sensitivity. There is little-to-no resolution in reconstructing m_H in these channels due to the presence of two neutrinos in the final state of the most sensitive analyses. Near $m_H = 2M_W$, the W bosons are on shell, and the kinematic variables take on different weights in the training of the MVA's than they do at masses even a bit above and below $2M_W$. At very high masses, the discriminating variable $\Delta R_{\rm leptons}$ plays much less of a role than it does near the W^+W^- threshold. We therefore expect a LEE factor of approximately two for the high-mass searches. In total, we expect that there are roughly four possible independent locations for uncorrelated excesses to appear in our analysis. The global p-value is therefore $1 - (1 - p_{\min})^4$, using the Dunn-Ŝidák correction [79].

m_H	obs	$-2\sigma \exp$	$-1\sigma \exp$	Median exp	$+1\sigma \exp$	$+2\sigma \exp$
(GeV/c^2)	(Limit/SM)	(Limit/SM)	(Limit/SM)	(Limit/SM)	(Limit/SM)	(Limit/SM)
100	1.19	0.51	0.68	0.93	1.28	1.74
105	1.34	0.52	0.70	0.98	1.37	1.89
110	1.81	0.54	0.74	1.06	1.52	2.16
115	2.25	0.61	0.83	1.16	1.62	2.24
120	2.86	0.68	0.91	1.28	1.80	2.51
125	2.89	0.74	0.99	1.39	1.96	2.74
130	2.94	0.79	1.04	1.46	2.05	2.87
135	2.58	0.75	1.03	1.45	2.05	2.83
140	2.32	0.73	0.99	1.36	1.89	2.58
145	1.32	0.64	0.88	1.23	1.73	2.39
150	0.89	0.59	0.79	1.10	1.55	2.16
155	0.81	0.46	0.68	0.97	1.35	1.84
160	0.50	0.37	0.50	0.71	0.99	1.38
165	0.41	0.36	0.49	0.67	0.93	1.26
170	0.84	0.44	0.58	0.81	1.13	1.57
175	0.99	0.50	0.69	0.97	1.36	1.89
180	1.21	0.64	0.82	1.12	1.59	2.24
185	1.72	0.72	1.00	1.41	1.99	2.76
190	2.31	0.95	1.28	1.77	2.46	3.38
195	4.44	1.14	1.49	2.06	2.87	3.98
200	4.46	1.23	1.64	2.30	3.24	4.52

TABLE III: CDF Run II Preliminary SM Higgs Combination, $L \leq 10.0 \text{ fb}^{-1}$. Limits are listed at the 95% C.L.

Therefore, we estimate that the global significance for the 2.6 σ level local excess in all search channels, using a LEE factor of 4, corresponds to 2.1 σ . The global significance for the 2.9 σ excess in the $H \to b\bar{b}$ channels, using a LEE factor of 2, is 2.7 σ . Since results from the LHC have excluded all but the range from 115.5 GeV to 127 GeV at the 95% CL, our LEE would only be 1 in this region, and the global p-value would equal the local p-value yielding a 2.9 σ significance. The excess in the CDF $H \to b\bar{b}$ channels has the highest global significance achieved to date from a Tevatron or LHC experiment.

In summary, we combine all available CDF results on SM Higgs boson searches, based on luminosities up to to 10.0 fb⁻¹. Compared to our previous combination, more integrated luminosity has been added to the existing channels, additional channels have been included, and analyses have been further optimized to gain sensitivity. We use the latest parton distribution functions and $gg \to H$ theoretical cross sections when comparing our limits to the SM predictions at high mass.

The 95% C.L. upper limits on Higgs boson production are a factor of 2.25 and 0.41 times the SM cross section for a Higgs boson mass of m_H =115 and 165 GeV/ c^2 , respectively. Based on simulation, the corresponding median expected upper limits are 1.16 and 0.67, respectively. Standard Model branching ratios, calculated as functions of the Higgs boson mass, are assumed.

We choose to use the intersections of piecewise linear interpolations of our observed and expected rate limits in order to quote ranges of Higgs boson masses that are excluded and that are expected to be excluded. The sensitivities of our searches to Higgs bosons are smooth functions of the Higgs boson mass and depend most strongly on the predicted cross sections and the decay branching ratios (the decay $H \to W^+W^-$ is the dominant decay for the region of highest sensitivity). The mass resolution of the channels is poor due to the presence of two highly energetic neutrinos in signal events. We therefore use the linear interpolations to extend the results from the 5 GeV/ c^2 mass grid investigated to points in between. This procedure yields higher expected and observed interpolated limits than if the full dependence of the cross section and branching ratio were included as well, since the latter produces limit curves that are concave upwards. The regions of Higgs boson masses excluded at the 95% C.L. thus obtained are $90 < m_H < 96.9 \text{ GeV}/c^2$, and $148.8 < m_H < 175.2 \text{ GeV}/c^2$. The expected exclusion region, given the current sensitivity, is $153.8 < m_H < 176.1 \text{ GeV}/c^2$, and $96.1 < m_H < 106 \text{ GeV}/c^2$. An excess in the observed data weakens

the expected limits. The largest excess at $m_H = 120$ GeV has a local p-value for a background fluctuation to produce the excess of $\sim 10^{-3}$, corresponding to a local significance of 2.6σ . The result is not unexpected as can be seen in our projection plots (Figure 10) which show the probability for the Tevatron finding 2σ and 3σ signals assuming 10 fb⁻¹ of data and all projected improvements incorporated. Figures ?? show how the projected improvements have been incorporated over the last few years, reaching almost to the bottom of the yellow band representing the sensitivity goal.

The global significance for a 2.6 σ excess anywhere in the full mass range is approximately 2.1σ . We also combine separately searches for $H \to b\bar{b}$ and $H \to W^+W^-$, and find that the excess is concentrated in the $H \to b\bar{b}$ channel. The global probability of the background to fluctuate to produce the 2.9 σ excess observed in the data at any mass in the $H \to b\bar{b}$ search region is estimated to be 2.7 σ . The excess in our $H \to b\bar{b}$ channels has the highest global significance for a Higgs signal achieved to date from a Tevatron or LHC experiment.

Acknowledgments

We thank the Fermilab staff and the technical staffs of the participating institutions for their vital contributions. 421 This work was supported by the U.S. Department of Energy and National Science Foundation; the Italian Istituto 422 Nazionale di Fisica Nucleare; the Ministry of Education, Culture, Sports, Science and Technology of Japan; the 423 Natural Sciences and Engineering Research Council of Canada; the National Science Council of the Republic of China; the Swiss National Science Foundation; the A.P. Sloan Foundation; the Bundesministerium für Bildung und 425 Forschung, Germany; the Korean World Class University Program, the National Research Foundation of Korea; the 426 Science and Technology Facilities Council and the Royal Society, UK; the Institut National de Physique Nucleaire et 427 Physique des Particules/CNRS; the Russian Foundation for Basic Research; the Ministerio de Ciencia e Innovación, 428 and Programa Consolider-Ingenio 2010, Spain; the Slovak R&D Agency; the Academy of Finland; and the Australian 429 Research Council (ARC).

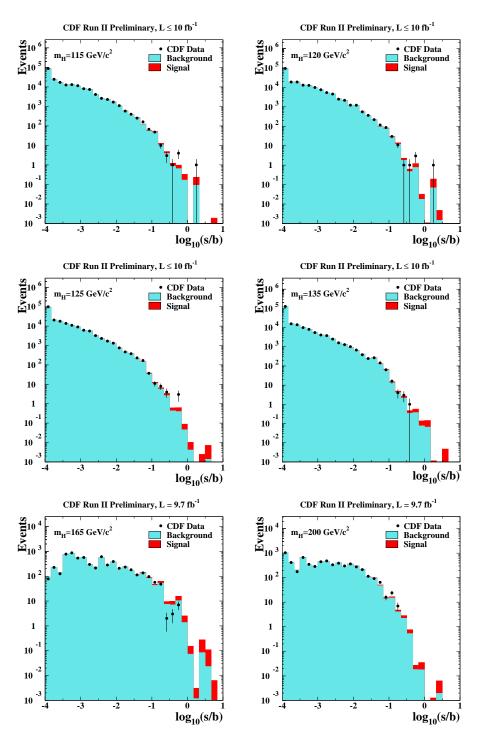


FIG. 1: Distributions of $\log_{10}(s/b)$, for the data from all contributing channels, for Higgs boson masses of 115, 120, 125, 135, 165, and 200 GeV/c^2 . The data are shown with points, and the expected signal is shown stacked on top of the backgrounds. Underflows and overflows are collected into the bottom and top bins.

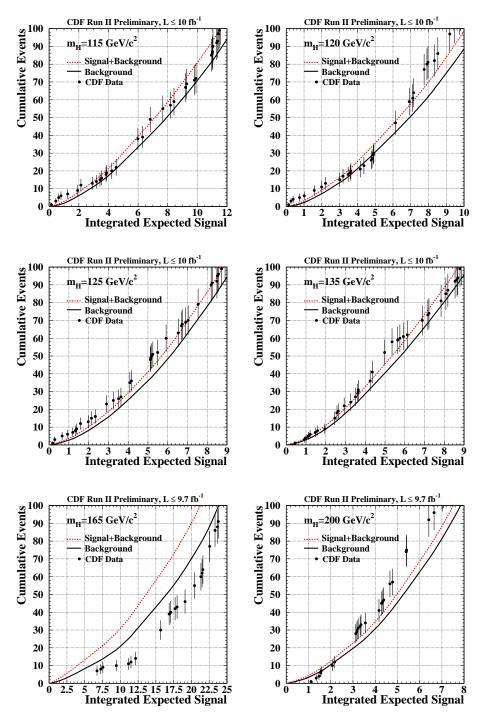


FIG. 2: Integrated distributions of s/b, starting at the high s/b side, for Higgs boson masses of 115, 120, 125, 135, 165, and 200 GeV/c^2 . The total signal+background and background-only integrals are shown separately, along with the data sums. Data are only shown for bins that have data events in them.

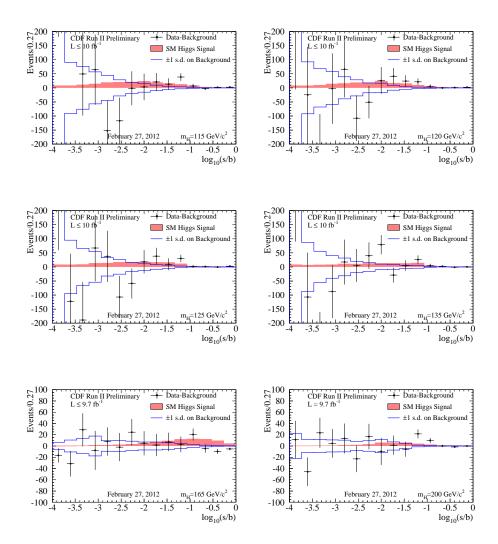


FIG. 3: These need to be updated. Background-subtracted data distributions for all channels, summed in bins of s/b, for Higgs boson masses of 115 and 165 ${\rm GeV}/c^2$. The background has been fit, within its systematic uncertainties, to the data. The points with error bars indicate the background-subtracted data; the sizes of the error bars are the square roots of the predicted background in each bin. The unshaded (blue-outline) histogram shows the systematic uncertainty on the best-fit background model, and the shaded histogram shows the expected signal for a Standard Model Higgs boson.

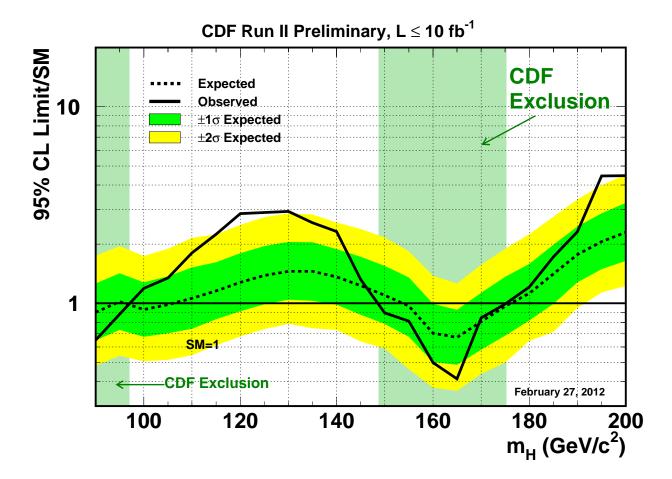


FIG. 4: Observed and expected (median, for the background-only hypothesis) 95% C.L. upper limits on the ratios to the SM cross section, as functions of the Higgs boson mass for the combined CDF and D0 analyses. The limits are expressed as a multiple of the SM prediction for test masses (every $5 \text{ GeV}/c^2$) for which both experiments have performed dedicated searches in different channels. The points are joined by straight lines for better readability. The bands indicate the 68% and 95% probability regions where the limits can fluctuate, in the absence of signal.

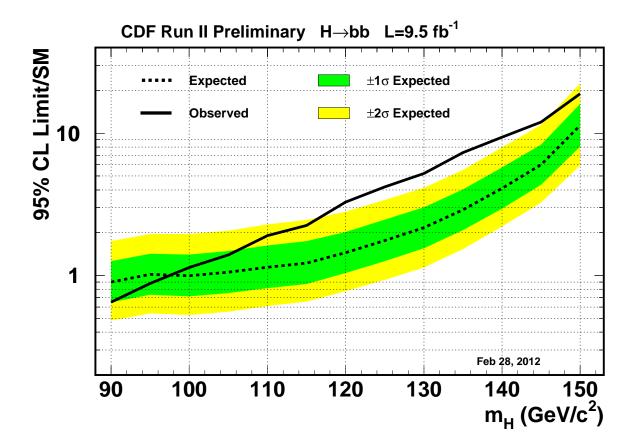


FIG. 5: Observed and expected (median, for the background-only hypothesis) 95% C.L. upper limits on the ratios to the SM cross section, as functions of the Higgs boson mass for the combination of CDF analyses focusing on the $H \to b\bar{b}$ decay channel. The limits are expressed as a multiple of the SM prediction for test masses (every 5 GeV/ c^2) for which both experiments have performed dedicated searches in different channels. The points are joined by straight lines for better readability. The bands indicate the 68% and 95% probability regions where the limits can fluctuate, in the absence of signal. The limits displayed in this figure are obtained with the Bayesian calculation.

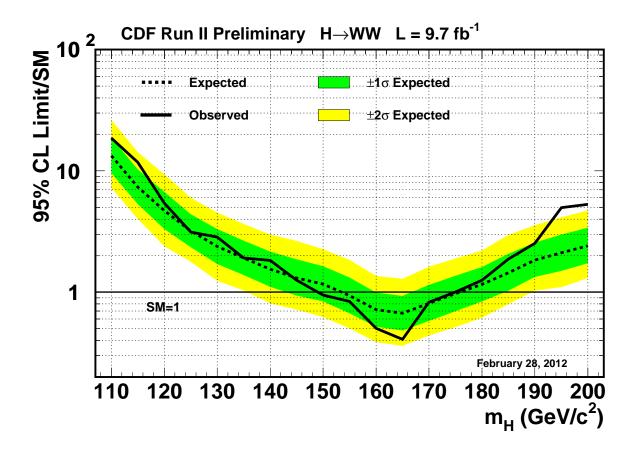


FIG. 6: Observed and expected (median, for the background-only hypothesis) 95% C.L. upper limits on the ratios to the SM cross section, as functions of the Higgs boson mass for the combination of CDF analyses focusing on the $H \to W^+W^-$ decay channel. The limits are expressed as a multiple of the SM prediction for test masses (every 5 GeV/c^2) for which both experiments have performed dedicated searches in different channels. The points are joined by straight lines for better readability. The bands indicate the 68% and 95% probability regions where the limits can fluctuate, in the absence of signal. The limits displayed in this figure are obtained with the Bayesian calculation.

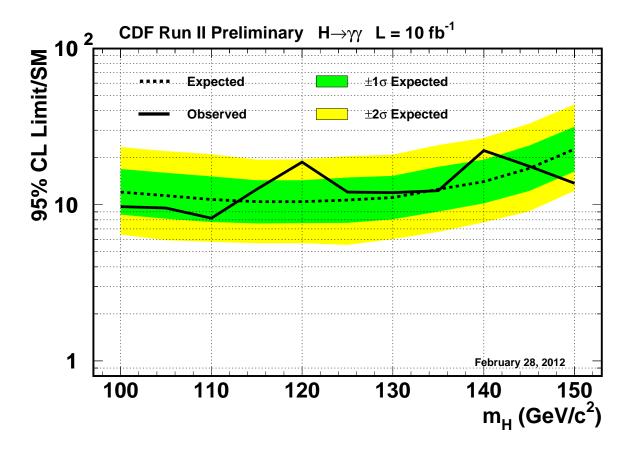


FIG. 7: Observed and expected (median, for the background-only hypothesis) 95% C.L. upper limits on the ratios to the SM cross section, as functions of the Higgs boson mass for the combination of CDF analyses focusing on the $H \to W^+W^-$ decay channel. The limits are expressed as a multiple of the SM prediction for test masses (every 5 GeV/ c^2) for which both experiments have performed dedicated searches in different channels. The points are joined by straight lines for better readability. The bands indicate the 68% and 95% probability regions where the limits can fluctuate, in the absence of signal. The limits displayed in this figure are obtained with the Bayesian calculation.

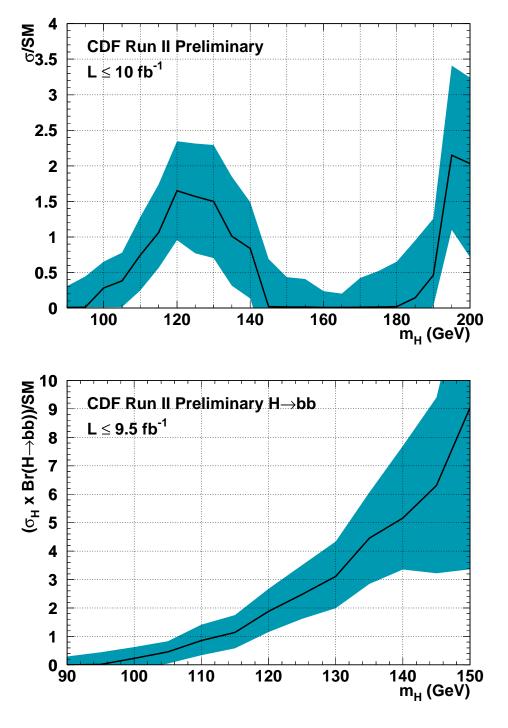


FIG. 8: Best fit signal cross sections, expressed as a ratio to the standard model Higgs cross section, calculated for all channels in the combination and for the subset of $H\to b\bar{b}$ channels. The band indicates the 1 σ uncertainty on the fit.

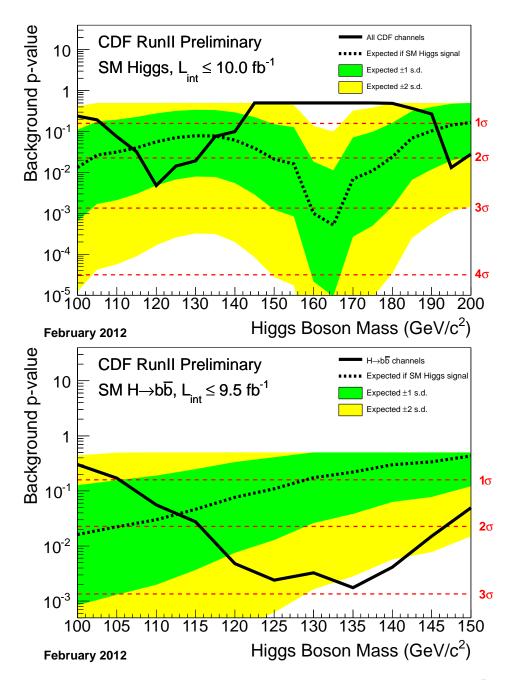
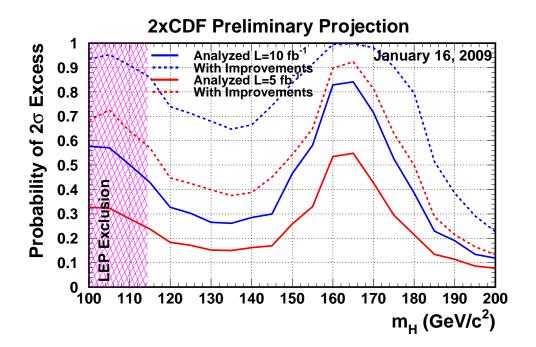


FIG. 9: Background p-value calculated for all channels in the combination and for the subset of $H \to b\bar{b}$ channels. The solid line represents the probability for a background model to produce the observed fitted cross section or larger. The dashed line represents the probability to fit a standard model Higgs cross section or larger. The colored bands represent the uncertainty on this probability due to statistical and systematic variations.



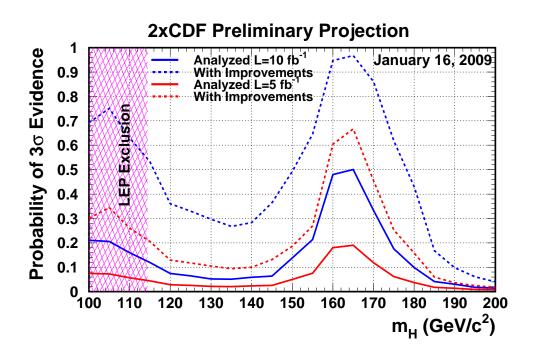
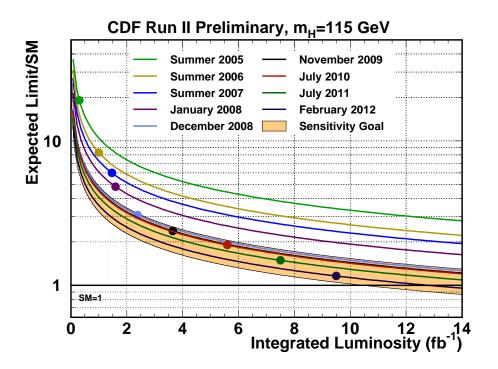


FIG. 10: Sensitivity projections as functions of m_H . These graphs show the chances of observing a 2σ excess (top) or a 3σ evidence (bottom), as functions of m_H , assuming a Higgs boson is present with production cross sections and decays at their SM values. CDF and D0 are assumed to contribute equally. The solid lines correspond to current performance as described in this note, and the dashed lines correspond to a performance level which corresponds to the bottom of the light orange bands in Figure 12. No account is taken of the data already collected and analyzed; existing excesses and deficits in the data do not affect these sensitivity projections. Two luminosity scenarios are considered: 5 fb⁻¹ of analyzed luminosity per experiment (red lines) and 10 fb⁻¹ of analyzed luminosity per experiment (blue lines).



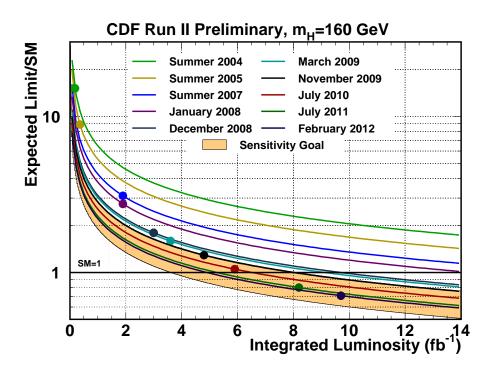
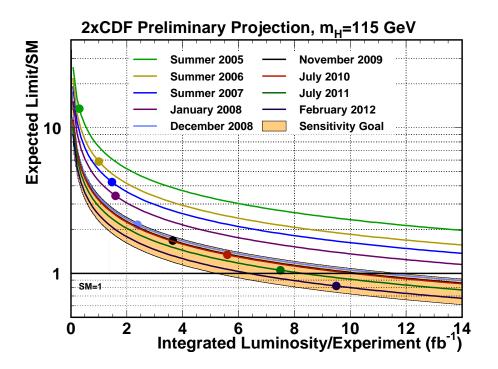


FIG. 11: Sensitivity projections and achieved sensitivities for the combined CDF Higgs boson searches, at $m_H=115$ and $160~{\rm GeV}/c^2$. The curves are proportional to $1/\sqrt{\int L dt}$ extrapolations of the median expected limits, and each analysis update corresponds to a new point with a new curve. The light orange bands indicate ranges of possible improvements in performance, relative to the Summer 2007 sensitivity. The top of the light orange bands is a factor of 1.5 below the Summer 2007 curve, and the bottom of the light orange bands are a further factor of 1.5 below the top of the light orange bands.



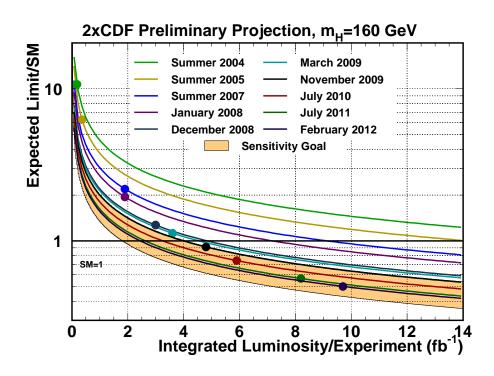


FIG. 12: Sensitivity projections and achieved sensitivities for the combined CDF Higgs boson searches, at $m_H=115$ and $160~{\rm GeV}/c^2$, with a multiplier of $1/\sqrt{2}$ applied to the expected limits, to approximate the contribution of D0, assuming identical performance. The curves are proportional to $1/\sqrt{\int L dt}$ extrapolations of the median expected limits, and each analysis update corresponds to a new point with a new curve. The light orange bands indicate ranges of possible improvements in performance, relative to the Summer 2007 sensitivity. The top of the light orange bands is a factor of 1.5 below the Summer 2007 curve, and the bottom of the light orange bands are a further factor of 1.5 below the top of the light orange bands. The points represent CDF's achieved sensitivities, where the expected limits have been divided by $\sqrt{2}$.

- [1] CDF Collaboration, "Measurement of the W Boson Mass using 2.2 fb⁻¹ of CDF II Data", CDF Conference Note 10775 (2012).
 - [2] D0 Collaboration, "Measurement of the W Boson Mass with the D0 Detector", arXiv:1203.0293v1[hep-ph].

433

434

435

436

437

438

439

440

441

442

443

444

448

449

450

451

452

453

454

457 458

459

460

462

463

464

465

466

467

- [3] The LEP Electroweak Working Group, "Status of March 2012", http://lepewwg.web.cern.ch/LEPEWWG/.
- [4] R. Barate et al. [LEP Working Group for Higgs boson searches], Phys. Lett. B 565, 61 (2003), [arXiv:hep-ex/0306033].
- [5] ATLAS Collaboration, "Combined search for the Standard Model Higgs Boson using up to 4.9 fb-1 of pp collision data at $\sqrt{s} = 7$ TeV with the ATLAS detector at the LHC", ATLAS-CONF-2011-163, arXiv:1202.1408 [hep-ex] (2012).
- [6] CMS Collaboration, "Combined results of searches for the standard model Higgs boson in pp collisions at $\sqrt{s} = 7$ TeV", CMS-PAS-HIG-11-032, arXiv:1202.1488 [hep-ex] (2012).
- [7] "Combined Upper Limits on Standard Model Higgs Boson Production from the D0 Experiment in up to 9.7 fb⁻¹ of data", D0 Conference Note 6304 (2012).
- [8] "Combined CDF and D0 searches for Standard Model Higgs Boson production with up to 10.0 fb⁻¹ of Data", CDF Note 10806, D0 Note 6303 (2012).
 - [9] CDF Collaboration, "Higgs optimized b-identification tagger at CDF", CDF Conference Note 10803 (2012).
- ⁴⁴⁵ [10] The CDF and D0 Collaborations and the TEVNPH Working Group, "Combined CDF and D0 Upper Limits on Standard Model Higgs Boson Production with up to 8.2 fb⁻¹ of Data,", FERMILAB-CONF-11-044-E, CDF Note 10441, D0 Note 6184, arXiv:1103.3233v1 [hep-ex] (2011);
 - The CDF and D0 Collaborations and the TEVNPH Working Group, "Combined CDF and D0 Upper Limits on Standard Model Higgs-Boson Production with up to 6.7 fb⁻¹ of Data", FERMILAB-CONF-10-257-E, CDF Note 10241, D0 Note 6096, arXiv:1007.4587v1 [hep-ex] (2010);
 - The CDF and D0 Collaborations and the TEVNPH Working Group, "Combined CDF and DZero Upper Limits on Standard Model Higgs-Boson Production with 2.1 to 4.2 fb⁻¹ of Data", FERMILAB-PUB-09-0557-E, CDF Note 9998, D0 Note 5983, arXiv:0911.3930v1 [hep-ex] (2009).
 - CDF Collaboration, "Search for $H \to WW^*$ Production Using 5.9 fb⁻¹", CDF Conference Note 10432 (2011);
- CDF Collaboration, "Combined Upper Limit on Standard Model Higgs Boson Production for ICHEP 2010", CDF Conference Note 10241 (2010);
 - CDF Collaboration, "Combined Upper Limit on Standard Model Higgs Boson Production for HCP 2009", CDF Conference Note 9999 (2009);
 - CDF Collaboration, "Combined Upper Limit on Standard Model Higgs Boson Production for Summer 2009", CDF Conference Note 9807 (2009);
 - [11] CDF Collaboration, "Inclusive Search for Standard Model Higgs Boson Production in the WW Decay Channel Using the CDF II Detector", Phys. Rev. Lett. 104, 061803 (2010);
 - The CDF and D0 Collaborations, "Combination of Tevatron Searches for the Standard Model Higgs Boson in the W^+W^- Decay Mode", Phys. Rev. Lett. 104, 061802 (2010).
 - [12] CDF Collaboration, "Measurement of WZ and ZZ production in final states with b-tagged jets", CDF Conference Note 10805 (2012).
- [13] CDF Collaboration, "Search for standard model Higgs boson production in association with a W boson using 9.4 fb⁻¹", CDF Conference Note 10796 (2012).
- 470 [14] CDF Collaboration, "Search for the standard model Higgs boson in the \rlap/E_T plus b-jets signature in 9.45 fb⁻¹", CDF Conference Note 10798 (2012).
- ⁴⁷² [15] CDF Collaboration, "A Search for the standard model Higgs boson in $ZH \to \ell^+\ell^-b\bar{b}$ with 9.45 fb⁻¹ of CDF II Data", CDF Conference Note 10799 (2012).
- ⁴⁷⁴ [16] CDF Collaboration, "Search for $H \to WW^*$ production using 9.7 fb⁻¹", CDF Conference Note 10785 (2012).
- ⁴⁷⁵ [17] CDF Collaboration, "Search for $H \to WW^*$ with leptons and hadronic taus in the final state using 9.7 fb⁻¹", CDF Conference Note 10781 (2012).
- 477 [18] CDF Collaboration, "An inclusive search for the Higgs boson in the four lepton final state", CDF Conference Note 10791 (2012).
- [19] CDF Collaboration, "Search for the standard model Higgs boson in $\tau^+\tau^-$ plus jets final state with 8.3 fb⁻¹ of CDF data", CDF Conference Note 10625 (2011).
- [20] CDF Collaboration, "Search for the standard model Higgs in the $\ell\nu\tau\tau$ and $\ell\ell\tau\tau$ channels", CDF Conference Note 10500 (2011).
- [21] CDF Collaboration, "A search for the Higgs boson in the all-hadronic channel using 9.45 fb⁻¹", CDF Conference Note 10792 (2012).

- ⁴⁸⁵ [22] CDF Collaboration, "Search for a standard model Higgs boson decaying into photons at CDF using 10.0 fb⁻¹ of data", CDF Conference Note 10737 (2012).
- ⁴⁸⁷ [23] CDF Collaboration, "Search for the Higgs boson produced in association with top quarks", CDF Conference Note 10801 (2012).
- 489 [24] CDF Collaboration, "Search for standard model Higgs boson production in association with $t\bar{t}$ using no lepton final state", CDF Conference Note 10582 (2011).
- ⁴⁹¹ [25] A. Hoecker, P. Speckmayer, J. Stelzer, J.Therhaag, E. von Toerne, and H. Voss, "TMVA 4 Toolkit for Multivariate Data Analysis with ROOT User's Guide" arXiv:physics/0703039a;
 - C. Cortes and V. Vapnik, "Support vector networks", Machine Learning 20, 273 (1995);
 - V. Vapnik, "The Nature of Statistical Learning Theory", Springer Verlag, New York (1995);
- C.J.C. Burges, "A Tutorial on Support Vector Machines for Pattern Recognition", Data Mining and Knowledge Discovery
 2, 1 (1998).
- ⁴⁹⁷ [26] C. Anastasiou, G. Dissertori, M. Grazzini, F. Stöckli and B. R. Webber, JHEP **0908**, 099 (2009).
- ⁴⁹⁸ [27] G. Bozzi, S. Catani, D. de Florian, and M. Grazzini, Phys. Lett. B **564**, 65 (2003);
 ⁴⁹⁹ G. Bozzi, S. Catani, D. de Florian, and M. Grazzini, Nucl. Phys. B **737**, 73 (2006).
 - [28] C. Balazs, J. Huston, I. Puljak, Phys. Rev. D 63 014021 (2001).
 C. Balazs and C.-P. Yuan, Phys. Lett. B 478 192-198 (2000).
 - Qing-Hong Cao and Chuan-Ren Chen, Phys. Rev. D 76 073006 (2007).
- ⁵⁰³ [29] C. Anastasiou, R. Boughezal and F. Petriello, JHEP **0904**, 003 (2009).
- ⁵⁰⁴ [30] D. de Florian and M. Grazzini, Phys. Lett. B **674**, 291 (2009).
 - [31] M. Grazzini, private communication (2010).

493

494

500

501

502

505

509

513

520

521

537

- 506 [32] The CDF and D0 Collaborations and the Tevatron Electroweak Working Group, arXiv:1007.3178 [hep-ex],
 507 arXiv:0903.2503 [hep-ex].
- ⁵⁰⁸ [33] I. W. Stewart, F. J. Tackmann, [arXiv:1107.2117 [hep-ph]].
 - [34] J. M. Campbell, R. K. Ellis, C. Williams, Phys. Rev. D81, 074023 (2010). [arXiv:1001.4495 [hep-ph]].
- 510 [35] R. V. Harlander and W. B. Kilgore, Phys. Rev. Lett. 88, 201801 (2002).
- [36] C. Anastasiou and K. Melnikov, Nucl. Phys. B **646**, 220 (2002).
- 512 [37] V. Ravindran, J. Smith, and W. L. van Neerven, Nucl. Phys. B 665, 325 (2003).
 - [38] S. Actis, G. Passarino, C. Sturm, and S. Uccirati, Phys. Lett. B 670, 12 (2008).
- 514 [39] U. Aglietti, R. Bonciani, G. Degrassi, A. Vicini, "Two-loop electroweak corrections to Higgs production in proton-proton collisions", arXiv:hep-ph/0610033v1 (2006).
- [40] S. Catani, D. de Florian, M. Grazzini and P. Nason, "Soft-gluon resummation for Higgs boson production at hadron colliders," JHEP 0307, 028 (2003) [arXiv:hep-ph/0306211].
- 518 [41] A. D. Martin, W. J. Stirling, R. S. Thorne and G. Watt, Eur. Phys. J. C 63, 189 (2009).
- $^{519}\quad [42]\ \mathtt{http://www.hep.ucl.ac.uk/pdf4lhc/};$
 - S. Alekhin et al., (PDF4LHC Working Group), [arXiv:1101.0536v1 [hep-ph]];
 - M. Botje et al., (PDF4LHC Working Group), [arXiv:1101.0538v1 [hep-ph]].
- ⁵²² [43] P. M. Nadolsky *et al.*, Phys. Rev. D **78**, 013004 (2008) [arXiv:0802.0007 [hep-ph]].
- [44] R. D. Ball *et al.* [NNPDF Collaboration], Nucl. Phys. B **809**, 1 (2009) [Erratum-ibid. B **816**, 293 (2009)] [arXiv:0808.1231 [hep-ph]].
- 525 [45] K. A. Assamagan *et al.* [Higgs Working Group Collaboration], "The Higgs working group: Summary report 2003," arXiv:hep-ph/0406152.
- ⁵²⁷ [46] O. Brein, A. Djouadi, and R. Harlander, Phys. Lett. B **579**, 149 (2004).
- 528 [47] M. L. Ciccolini, S. Dittmaier, and M. Kramer, Phys. Rev. D 68, 073003 (2003).
- ⁵²⁹ [48] E. Berger and J. Campbell, Phys. Rev. D **70** 073011 (2004).
- [49] W. Beenaker, S. Dittmaier, M. Krämer, B. Plümper, M. Spira, and P. M. Zerwas, Phys. Rev. Lett. 87, 201805 (2001);
 L. Reina and S. Dawson, Phys. Rev. Lett. 87, 201804 (2001).
- $_{532}$ [50] J. Baglio and A. Djouadi, arXiv:1003.4266 [hep-ph] (2010). We have obtained extended versions of the table of WH and ZH cross sections for all Higgs boson masses we test, and with more digits of precision, from the authors.
- 534 [51] The Fortran program can be found on Michael Spira's web page http://people.web.psi.ch/~mspira/proglist.html.
- ⁵³⁵ [52] O. Brein, A. Djouadi, and R. Harlander, Phys. Lett. B **579**, 149 (2004).
- 536 [53] M. L. Ciccolini, S. Dittmaier, and M. Kramer, Phys. Rev. D **68**, 073003 (2003).
 - [54] P. Bolzoni, F. Maltoni, S.-O. Moch, and M. Zaro, Phys. Rev. Lett. 105, 011801 (2010) [arXiv:1003.4451v2 [hep-ph]].
- [55] M. Ciccolini, A. Denner, and S. Dittmaier, Phys. Rev. Lett. 99, 161803 (2007) [arXiv:0707.0381 [hep-ph]];
 M. Ciccolini, A. Denner, and S. Dittmaier, Phys. Rev. D 77, 013002 (2008) [arXiv:0710.4749 [hep-ph]].
- We would like to thank the authors of the HAWK program for adapting it to the Tevatron.

- 541 [56] T. Sjöstrand, L. Lonnblad and S. Mrenna, "PYTHIA 6.2: Physics and manual," arXiv:hep-ph/0108264.
- ⁵⁴² [57] H. L. Lai et al., Phys. Rev D **55**, 1280 (1997).

546

549

559

560

- ⁵⁴³ [58] S. Dittmaier et al. [LHC Higgs Cross Section Working Group Collaboration], [arXiv:1101.0593 [hep-ph]].
- ⁵⁴⁴ [59] A. Djouadi, J. Kalinowski and M. Spira, Comput. Phys. Commun. **108**, 56 (1998).
- 545 [60] A. Bredenstein, A. Denner, S. Dittmaier, and M. M. Weber, Phys. Rev. D 74, 013004 (2006);
 - A. Bredenstein, A. Denner, S. Dittmaier, and M. Weber, JHEP 0702, 080 (2007);
- A. Bredenstein, A. Denner, S. Dittmaier, A. Mück, and M. M. Weber, JHEP **0702**, 080 (2007) http://omnibus.uni-freiburg.de/~sd565/programs/prophycey4f/prophecy4f.html (2010).
 - [61] J. Baglio, A. Djouadi, JHEP **1103**, 055 (2011). [arXiv:1012.0530 [hep-ph]].
- 550 [62] A. Denner, S. Heinemeyer, I. Puljak, D. Rebuzzi and M. Spira, Eur. Phys. J. C 71, 1753 (2011) [arXiv:1107.5909 [hep-ph]].
- [63] M. L. Mangano, M. Moretti, F. Piccinini, R. Pittau and A. D. Polosa, "ALPGEN, a generator for hard multiparton processes in hadronic collisions," JHEP 0307, 001 (2003).
- ⁵⁵³ [64] S. Frixione and B.R. Webber, JHEP **0206**, 029 (2002).
- ⁵⁵⁴ [65] G. Corcella *et al.*, JHEP **0101**, 010 (2001).
- 555 [66] A. Pukhov *et al.*, "CompHEP: A package for evaluation of Feynman diagrams and integration over multi-particle phase 556 space. User's manual for version 33," [arXiv:hep-ph/9908288].
- 557 [67] J. Campbell and R. K. Ellis, http://mcfm.fnal.gov/.
- ⁵⁵⁸ [68] T. Junk, Nucl. Instrum. Meth. A **434**, 435 (1999);
 - A.L. Read, "Modified Frequentist analysis of search results (the CL_s method)", in F. James, L. Lyons and Y. Perrin (eds.), Workshop on Confidence Limits, CERN, Yellow Report 2000-005, available through cdsweb.cern.ch.
- ⁵⁶¹ [69] W. Fisher, "Systematics and Limit Calculations," FERMILAB-TM-2386-E.
- ⁵⁶² [70] S. Moch and P. Uwer, U. Langenfeld, S. Moch and P. Uwer, Phys. Rev. D **80**, 054009 (2009).
- [71] The CDF and D0 Collaborations and the Tevatron Electroweak Working Group, arXiv:0903.2503 [hep-ex].
- [72] M. Cacciari, S. Frixione, M. L. Mangano, P. Nason and G. Ridolfi, JHEP 0809, 127 (2008).
 N. Kidonakis and R. Vogt, Phys. Rev. D 78, 074005 (2008).
- ⁵⁶⁶ [73] N. Kidonakis, Phys. Rev. D **74**, 114012 (2006).
- ⁵⁶⁷ [74] N. Kidonakis, private communication.
- ⁵⁶⁸ [75] N. Kidonakis, arXiv:1005.3330 [hep-ph].
- 9 [76] B. W. Harris, E. Laenen, L. Phaf, Z. Sullivan and S. Weinzierl, Phys. Rev. D 66, 054024 (2002).
- ⁵⁷⁰ [77] J. Campbell and R. K. Ellis, Phys. Rev. D **65**, 113007 (2002).
- ⁵⁷¹ [78] E. Gross and O. Vitells, Eur. Phys. J. C **70**, 525 (2010) [arXiv:1005.1891 [physics.data-an]].
- [79] Dunn, O.J., "Multiple Comparisons Among Means" Journal of the American Statistical Association, 56, 52-64 (1961).

573 Appendices

APPENDIX A: SYSTEMATIC UNCERTAINTIES

TABLE IV: Systematic uncertainties on the signal and background contributions for CDF's $WH \to \ell\nu b\bar{b}$ two tight b-tag (TT), one tight b-tag and one loose b-tag (TL), and two loose b-tag (LL) channels. Systematic uncertainties are listed by name; see the original references for a detailed explanation of their meaning and on how they are derived. Systematic uncertainties for WH shown in this table are obtained for $m_H = 115~{\rm GeV}/c^2$. Uncertainties are relative, in percent, and are symmetric unless otherwise indicated. Shape uncertainties are labeled with an "S".

CDF: two tight b-tag (TT) $WH \rightarrow \ell\nu b\bar{b}$ channel relative uncertainties (%)

Contribution	$W + \mathrm{HF}$	Mistags	Top	Diboson	$\operatorname{Non-}W$	WH
Luminosity $(\sigma_{\text{inel}}(p\bar{p}))$	3.8	0	3.8	3.8	0	3.8
Luminosity Monitor	4.4	0	4.4	4.4	0	4.4
Lepton ID	2.0 - 4.5	0	2.0 - 4.5	2.0 - 4.5	0	2.0 - 4.5
Jet Energy Scale	4.0 - 16.6(S)	0.9 - 3.3(S)	0.9 - 10.4(S)	4.7-19.7(S)	0	2.3-13.6(S)
Mistag Rate (tight)	0	40	0	0	0	0
Mistag Rate (loose)	0	0	0	0	0	0
B-Tag Efficiency (tight)	0	0	7.8	7.8	0	7.8
B-Tag Efficiency (loose)	0	0	0	0	0	0
$t\bar{t}$ Cross Section	0	0	10	0	0	0
Diboson Rate	0	0	0	6.0	0	0
Signal Cross Section	0	0	0	0	0	5
HF Fraction in W+jets	30	0	0	0	0	0
ISR+FSR+PDF	0	0	0	0	0	6.4 - 12.6
Q^2	4.0-8.8(S)	0.9 - 1.8(S)	0	0	0	0
QCD Rate	0	0	0	0	40	0

CDF: one tight and one loose b-tag (TL) $WH \to \ell \nu b \bar{b}$ channel relative uncertainties (%)

Contribution	$W+{\rm HF}$	Mistags	Top	Diboson	Non-W	WH
Luminosity $(\sigma_{\text{inel}}(p\bar{p}))$	3.8	0	3.8	3.8	0	3.8
Luminosity Monitor	4.4	0	4.4	4.4	0	4.4
Lepton ID	2.0 - 4.5	0	2.0 - 4.5	2.0 - 4.5	0	2.0 - 4.5
Jet Energy Scale	3.9-12.4(S)	0.9 - 3.3(S)	1.4 - 11.5(S)	5.0 - 16.0(S)		2.5 - 16.1(S)
Mistag Rate (tight)	0	19	0	0	0	0
Mistag Rate (loose)	0	10	0	0	0	0
B-Tag Efficiency (tight)	0	0	3.9	3.9	0	3.9
B-Tag Efficiency (loose)	0	0	3.2	3.2	0	3.2
$t\bar{t}$ Cross Section	0	0	10	0	0	0
Diboson Rate	0	0	0	6.0	0	0
Signal Cross Section	0	0	0	0	0	5
HF Fraction in W+jets	30	0	0	0	0	0
ISR+FSR+PDF	0	0	0	0	0	3.3-10.3
Q^2	3.9-7.7(S)	0.9 - 1.9(S)	0	0	0	0
QCD Rate	0	0	0	0	40	0

CDF: two loose b-tag (LL) $WH \to \ell \nu b \bar{b}$ channel relative uncertainties (%)

Contribution	$W+{\rm HF}$	Mistags	Top	Diboson	$\operatorname{Non-}W$	WH
Luminosity $(\sigma_{\text{inel}}(p\bar{p}))$	3.8	0	3.8	3.8	0	3.8
Luminosity Monitor	4.4	0	4.4	4.4	0	4.4
Lepton ID	2	0	2	2	0	2
Jet Energy Scale	3.6-6.9(S)	0.9 - 1.8(S)	1.7-7.9(S)	1.2 - 8.5	0	2.7-5.4(S)
Mistag Rate (tight)	0	0	0	0	0	0
Mistag Rate (loose)	0	20	0	0	0	0
B-Tag Efficiency (tight)	0	0	0	0	0	0
B-Tag Efficiency (loose)	0	0	6.3	6.3	0	6.3
$t\bar{t}$ Cross Section	0	0	10	0	0	0
Diboson Rate	0	0	0	6.0	0	0
Signal Cross Section	0	0	0	0	0	10
HF Fraction in W+jets	30	0	0	0	0	0
ISR+FSR+PDF	0	0	0	0	0	2.0 - 13.6
QCD Rate	3.6-6.9(S)	0.9 - 1.8(S)	0	0	40	0

TABLE V: Systematic uncertainties on the signal and background contributions for CDF's $WH \to \ell\nu b\bar{b}$ single tight b-tag (Tx) and single loose b-tag (Lx) categories. Systematic uncertainties are listed by name; see the original references for a detailed explanation of their meaning and on how they are derived. Systematic uncertainties for WH shown in this table are obtained for $m_H = 115~{\rm GeV}/c^2$. Uncertainties are relative, in percent, and are symmetric unless otherwise indicated. Shape uncertainties are labeled with an "S".

CDF: single tight b-tag (Tx) $WH \to \ell \nu b\bar{b}$ channel relative uncertainties (%)

Contribution	$W{+}\mathrm{HF}$	Mistags	Тор	Diboson	$\operatorname{Non-}W$	WH
Luminosity $(\sigma_{\text{inel}}(p\bar{p}))$	3.8	0	3.8	3.8	0	3.8
Luminosity Monitor	4.4	0	4.4	4.4	0	4.4
Lepton ID	2.0 - 4.5	0	2.0 - 4.5	2.0 - 4.5	0	2.0 - 4.5
Jet Energy Scale	3.2-6.9(S)	0.9 - 1.8(S)	0.8-9.7(S)	3.6-13.2(S)	0	3.0-5.0(S)
Mistag Rate (tight)	0	19	0	0	0	0
Mistag Rate (loose)	0	0	0	0	0	0
B-Tag Efficiency (tight)	0	0	3.9	3.9	0	3.9
B-Tag Efficiency (loose)	0	0	0	0	0	0
$t\bar{t}$ Cross Section	0	0	10	0	0	0
Diboson Rate	0	0	0	6.0	0	0
Signal Cross Section	0	0	0	0	0	5
HF Fraction in W+jets	30	0	0	0	0	0
ISR+FSR+PDF	0	0	0	0	0	3.8 - 6.8
Q^2	3.2-6.9(S)	0.9 - 1.8(S)	0	0	0	0
QCD Rate	0	0	0	0	40	0

CDF: single loose b-tag (Lx) $WH \rightarrow \ell \nu b \bar{b}$ channel relative uncertainties (%)

Contribution	$W{+}\mathrm{HF}$	Mistags	Top	Diboson	$\mathrm{Non}\text{-}W$	WH
Luminosity $(\sigma_{\text{inel}}(p\bar{p}))$	3.8	0	3.8	3.8	0	3.8
Luminosity Monitor	4.4	0	4.4	4.4	0	4.4
Lepton ID	2	0	2	2	0	2
Jet Energy Scale	2.2-6.0(S)	0.9 - 1.8(S)	1.6-8.6(S)	4.6-9.6(S)	0	3.1-4.8(S)
Mistag Rate (tight)	0	0	0	0	0	0
Mistag Rate (loose)	0	10	0	0	0	0
B-Tag Efficiency (tight)	0	0	0	0	0	0
B-Tag Efficiency (loose)	0	0	3.2	3.2	0	3.2
$t\bar{t}$ Cross Section	0	0	10	0	0	0
Diboson Rate	0	0	0	6.0	0	0
Signal Cross Section	0	0	0	0	0	10
HF Fraction in W+jets	30	0	0	0	0	0
ISR+FSR+PDF	0	0	0	0	0	2.4-4.9
QCD Rate	2.1-6.0(S)	0.9 - 1.8(S)	0	0	40	0

TABLE VI: Systematic uncertainties on the signal and background contributions for CDF's $WH, ZH \to \rlap/E_T b\bar{b}$ tight double tag (SS), loose double tag (SJ), and single tag (1S) channels. Systematic uncertainties are listed by name; see the original references for a detailed explanation of their meaning and on how they are derived. Systematic uncertainties for ZH and WH shown in this table are obtained for $m_H = 120~{\rm GeV}/c^2$. Uncertainties are relative, in percent, and are symmetric unless otherwise indicated. Shape uncertainties are labeled with an "S".

CDF: tight double-tag (SS) $WH,ZH\to E_T b\bar{b}$ channel relative uncertainties (%)

Contribution	ZH	WH	Multijet	Mistags	Top Pair	S. Top	Diboson	W + HF	Z + HF
Luminosity	3.8	3.8	-	-	3.8	3.8	3.8	3.8	3.8
Lumi Monitor	4.4	4.4			4.4	4.4	4.4	4.4	4.4
Tagging SF	10.4	10.4			10.4	10.4	10.4	10.4	10.4
Trigger Eff. (S)	0.9	1.4	0.9		0.9	1.6	2.0	1.8	1.2
Lepton Veto	2.0	2.0			2.0	2.0	2.0	2.0	2.0
PDF Acceptance	3.0	3.0			3.0	3.0	3.0	3.0	3.0
JES (S)	$^{+1.7}_{-1.8}$	$^{+2.4}_{-2.3}$			$^{+0.0}_{-0.1}$	$^{+2.5}_{-2.4}$	$^{+4.1}_{-4.5}$	$^{+4.3}_{-4.6}$	$^{+8.8}_{-3.2}$
ISR/FSR	+:	3.0 3.0			0.1	2.1	1.0	1.0	0.2
Cross-Section	5	5			10	10	6	30	30
Multijet Norm. (shape)			2.5						
Mistag (S)				+36.7 -30					

CDF: loose double-tag (SJ) $WH, ZH \rightarrow E_T b\bar{b}$ channel relative uncertainties (%)

Contribution	ZH	WH	Multijet	Mistags	Top Pair	S. Top	Diboson	W + HF	Z + HF
Luminosity	3.8	3.8	-	-	3.8	3.8	3.8	3.8	3.8
Lumi Monitor	4.4	4.4			4.4	4.4	4.4	4.4	4.4
Tagging SF	8.3	8.3			8.3	8.3	8.3	8.3	8.3
Trigger Eff. (S)	1.2	1.7	1.6		0.9	1.8	2.0	2.5	1.9
Lepton Veto	2.0	2.0			2.0	2.0	2.0	2.0	2.0
PDF Acceptance	3.0	3.0			3.0	3.0	3.0	3.0	3.0
JES (S)	$^{+1.9}_{-1.9}$	$^{+2.4}_{-2.4}$			$^{+3.0}_{-2.8}$	-0.6 0.2	$^{+4.2}_{-4.2}$	$^{+6.8}_{-5.9}$	$^{+8.3}_{-3.1}$
ISR/FSR	+2	2.4 2.4			2.0	0.2	1.2	0.0	0.1
Cross-Section	5.0	5.0			10	10	6	30	30
Multijet Norm.			1.6						
Mistag (S)				$+65.2 \\ -38.5$					

CDF: single-tag (1S) $WH, ZH \to E_T b\bar{b}$ channel relative uncertainties (%)

Contribution	ZH	WH	Multijet	Mistags	Top Pair	S. Top	Diboson	W + HF	Z + HF
Luminosity	3.8	3.8			3.8	3.8	3.8	3.8	3.8
Lumi Monitor	4.4	4.4			4.4	4.4	4.4	4.4	4.4
Tagging SF	5.2	5.2			5.2	5.2	5.2	5.2	5.2
Trigger Eff. (S)	1.2	1.7	1.6		0.9	1.8	2.0	2.5	1.9
Lepton Veto	2.0	2.0			2.0	2.0	2.0	2.0	2.0
PDF Acceptance	3.0	3.0			3.0	3.0	3.0	3.0	3.0
JES (S)	$^{+2.6}_{-2.6}$	$^{+3.3}_{-3.1}$			$-0.8 \\ +0.6$	$^{+2.7}_{-2.8}$	$^{+5.1}_{-5.1}$	$^{+8.2}_{-6.8}$	$^{+10.8}_{-3.4}$
ISR/FSR	+:	2.0 2.0			10.0	2.0	0.1	0.0	0.1
Cross-Section	5.0	5.0			10	10	6	30	30
Multijet Norm.			0.7						
Mistag (S)				$^{+17.9}_{-17.4}$					

TABLE VII: Systematic uncertainties on the signal and background contributions for CDF's $ZH \to \ell^+\ell^-b\bar{b}$ tight double tag (TT) and one tight tag and one loose tag (TL) channels. Systematic uncertainties are listed by name; see the original references for a detailed explanation of their meaning and on how they are derived. Uncertainties are relative, in percent on the event yield. Shape uncertainties are labeled with an "(S)".

CDF: tight double tag (TT) $\ell\ell b\bar{b}$ channels relative uncertainties (%)

Contribution	Fakes	$tar{t}$	WW	WZ	ZZ	$Z + c\bar{c}$	$Z+bar{b}$	Mistags	ZH
Luminosity $(\sigma_{\text{inel}}(p\bar{p}))$	rakes	3.8	3.8	3.8	3.8	$\frac{2+cc}{3.8}$	$\frac{2+60}{3.8}$	Mistags	3.8
Luminosity $(\sigma_{\text{inel}}(pp))$ Luminosity Monitor		4.4	4.4	4.4	4.4	4.4	4.4		4.4
v									
Lepton ID		1	1	1	1	1	1		1
Lepton Energy Scale	.	1.5	1.5	1.5	1.5	1.5	1.5		1.5
Fake $Z \to e^+e^-$	50								
Fake $Z \to \mu^+ \mu^-$	5								
Tight Mistag Rate								40	
Loose Mistag Rate									
JES $[e^+e^-, 2 \text{ jet}]$		$^{+0.8}_{-0.7}$	$^{+14.4}_{-13.2}$	$^{+6.2}_{-6.2}$	$^{+8.2}_{-8.3}$	$^{+5.6}_{-5.6}$	+8.1 -7.9	+10.4 -10.4	+3.6 -4.2
JES $[e^+e^-, 3 \text{ jet}]$		$^{-0.7}_{+8.3}$	$^{-13.2}_{-0.7}$	$\begin{array}{c} -6.2 \\ -4.2 \\ \pm 4.3 \end{array}$	+14.4	+10.6	$-7.9 \\ +13.2 \\ -13.2$	$-10.4 \\ +12.4 \\ -12.4$	$^{-4.2}_{+15.1}$
JES $[\mu^+\mu^-, 2 \text{ jet}]$		$^{-8.2}_{+1.0}$	$^{+1.7}_{+5.4}$	$^{+4.3}_{+13.4}$ $^{-13.4}$	$^{-13.3}_{+7.7}$ $^{-7.7}$	$^{-10.5}_{-1.5}$	$^{-13.2}_{+8.2}$ $^{-8.2}$	$^{-12.4}_{+5.7}$ $^{-5.8}$	$^{-14.9}_{+3.1}$ $^{-3.5}$
JES $[\mu^+\mu^-, 3 \text{ jet}]$		$^{-0.9}_{+9.3}$	$^{+2.1}_{+3.9}$	+4.8	+15.5	$^{+1.5}_{+7.3}$	+14.2	+20.5	+12.5
Tight b -tag Rate		$^{-9.1}_{7.8}$	$^{-3.0}_{7.8}$	$^{-5.7}$	$^{-15.5}_{7.8}$	$\begin{array}{c} -7.3 \\ 7.8 \end{array}$	$^{-14.5}$ 7.8	-18.0	$^{-13.3}$ 7.8
Loose b-tag Rate		1.0	1.0	1.0	1.0	1.0	1.0		1.0
$t\bar{t}$ Cross Section		10							
Diboson Cross Section		10	6	6	6				
			O	O	O	40	40		
Z+HF Cross Section						40	40		-
ZH Cross Section									5
ISR/FSR									5.5 - 7.6
Electron Trigger Eff.		1	1	1	1	1	1		1
Muon Trigger Eff.		5	5	5	5	5	5		5

CDF: one tight and one loose tag (TL) $\ell\ell b\bar{b}$ channels relative uncertainties (%)

G	D 1	. =	*****	117.77		7	7 . 1 <u>7</u>	3.61	7.11
Contribution	Fakes	$t\bar{t}$	WW	WZ	ZZ	$Z + c\bar{c}$	Z + bb	Mistags	ZH
Luminosity $(\sigma_{\text{inel}}(p\bar{p}))$		3.8	3.8	3.8	3.8	3.8	3.8		3.8
Luminosity Monitor		4.4	4.4	4.4	4.4	4.4	4.4		4.4
Lepton ID		1	1	1	1	1	1		1
Lepton Energy Scale		1.5	1.5	1.5	1.5	1.5	1.5		1.5
Fake $Z \to e^+ e^-$	50								
Fake $Z \to \mu^+ \mu^-$	5								
Tight Mistag Rate								19	
Loose Mistag Rate								10	
JES $[e^+e^-, 2 \text{ jet}]$		$^{+0.9}_{-1.0}$	$^{+13.0}_{-12.6}$	$^{+9.3}_{-9.4}$	$^{+10.3}_{-10.2}$	$^{+10.3}_{-10.3}$	$^{+8.9}_{-9.3}$	$^{+10.4}_{-10.4}$	$^{+4.0}_{-4.2}$
JES $[e^+e^-, 3 \text{ jet}]$		$^{+6.9}_{-7.0}$	$^{+10.3}_{-8.3}$	$^{+16.2}_{-16.0}$	$^{+14.6}_{-14.5}$	$^{+22.8}_{-23.4}$	$^{+15.1}_{-15.2}$	$^{+18.5}_{-18.5}$	$^{+14.3}_{-14.4}$
JES $[\mu^+\mu^-, 2 \text{ jet}]$		$^{+1.1}_{-1.1}$	+3.7	$^{+6.5}_{-6.5}$	+7.5 -7.5	$+12.5 \\ -12.4$	$+10.1 \\ -10.1$	$^{+11.0}_{-11.0}$	+4.0 -4.1
JES $[\mu^+\mu^-, 3 \text{ jet}]$		$+8.0 \\ -8.0$	$^{1.8}_{+2.0}_{-1.6}$	$^{+14.4}_{-14.5}$	$^{+24.1}_{-24.1}$	$^{+16.0}_{-14.7}$	$+17.5 \\ -17.6$	$+14.3 \\ -14.2$	$+13.1 \\ -14.0$
Tight b-tag Rate		$\frac{-3.0}{3.9}$	$3.9^{-1.0}$	$3.9^{-14.5}$	3.9	$3.9^{-14.7}$	3.9	-14.2	$3.9^{-14.0}$
Loose b-tag Rate		3.2	3.2	3.2	3.2	3.2	3.2		3.2
$t\bar{t}$ Cross Section		10							
Diboson Cross Section			6	6	6				
Z+HF Cross Section						40	40		
ZH Cross Section									5
ISR/FSR									3.4 - 7.0
Electron Trigger Eff.		1	1	1	1	1	1		1
Muon Trigger Eff.		5	5	5	5	5	5		5

TABLE VIII: Systematic uncertainties on the signal and background contributions for CDF's $ZH \to \mu^+\mu^-b\bar{b}$ single tight tag (Tx) and double loose tag (LL) channels. Systematic uncertainties are listed by name; see the original references for a detailed explanation of their meaning and on how they are derived. Uncertainties are relative, in percent on the event yield. Shape uncertainties are labeled with an "(S)".

CDF: single tight tag (TT) $\ell\ell b\bar{b}$ channels relative uncertainties (%)

C	D.I	, , -	******	111.77		7	σ , $\iota \bar{\iota}$	3.61	7.11
Contribution	Fakes	$t \bar{t}$	WW	WZ	ZZ	$Z + c\bar{c}$	Z + bb	Mistags	ZH
Luminosity $(\sigma_{\rm inel}(p\bar{p}))$		3.8	3.8	3.8	3.8	3.8	3.8		3.8
Luminosity Monitor		4.4	4.4	4.4	4.4	4.4	4.4		4.4
Lepton ID		1	1	1	1	1	1		1
Lepton Energy Scale		1.5	1.5	1.5	1.5	1.5	1.5		1.5
Fake $Z \to e^+e^-$	50								
Fake $Z \to \mu^+ \mu^-$	5								
Tight Mistag Rate								19	
Loose Mistag Rate									
JES $[e^+e^-, 2 \text{ jet}]$		$-0.3 \\ +0.3$	$^{+13.7}_{-13.5}$	$^{+8.5}_{-8.5}$	$^{+6.5}_{-6.3}$	$^{+13.2}_{-13.2}$	$+11.0 \\ -11.1$	$^{+12.0}_{-12.0}$	+3.5 -3.8
JES $[e^+e^-, 3 \text{ jet}]$		$^{+0.3}_{-7.1}$	$^{-13.5}_{+8.9}$	$^{-8.5}_{+17.0}_{-17.0}$	$^{-6.3}_{+15.4}$	$^{-13.2}_{+16.4}$	$^{-11.1}_{+15.8}$	$^{-12.0}_{+18.6}$	$-3.8 \\ +15.4 \\ -15.7$
JES $[\mu^+\mu^-, 2 \text{ jet}]$		$^{-7.1}_{+0.6}$ $^{-0.7}$	$^{-8.2}_{+3.9}_{-3.3}$	+8.6 -8.6	$^{-15.4}_{+7.6}$ $^{-7.7}$	$^{-16.4}_{+10.2}$ $^{-10.5}$	$^{-15.9}_{+9.3}$ $^{-9.3}$	$^{-18.5}_{+11.1}_{-11.1}$	$^{-15.7}_{+3.4}_{-3.7}$
JES $[\mu^+\mu^-, 3 \text{ jet}]$		$+5.5 \\ -5.5$	$^{+5.7}_{-1.9}$	$^{+16.6}_{-16.6}$	$^{+16.8}_{-16.8}$	$^{+16.1}_{-16.2}$	$^{+16.1}_{-16.2}$	$+17.5 \\ -17.5$	$^{+13.8}_{-13.9}$
Tight b-tag Rate		3.9	3.9	3.9	3.9	3.9	3.9	1110	3.9
Loose b-tag Rate									
$t\bar{t}$ Cross Section		10							
Diboson Cross Section			6	6	6				
Z+HF Cross Section						40	40		
ZH Cross Section									5
ISR/FSR									0.9 – 12.8
Electron Trigger Eff.		1	1	1	1	1	1		1
Muon Trigger Eff.		5	5	5	5	5	5		5

CDF: double loose tag (LL) $\ell\ell b\bar{b}$ channels relative uncertainties (%)

~		. =	*****			.	.	3.60	
Contribution	Fakes	$t \bar{t}$	WW	WZ	ZZ	$Z + c\bar{c}$	Z + bb	Mistags	ZH
Luminosity $(\sigma_{\text{inel}}(p\bar{p}))$		3.8	3.8	3.8	3.8	3.8	3.8		3.8
Luminosity Monitor		4.4	4.4	4.4	4.4	4.4	4.4		4.4
Lepton ID		1	1	1	1	1	1		1
Lepton Energy Scale		1.5	1.5	1.5	1.5	1.5	1.5		1.5
Fake $Z \to e^+ e^-$	50								
Fake $Z \to \mu^+ \mu^-$	5								
Tight Mistag Rate									
Loose Mistag Rate								20	
JES $[e^+e^-, 2 \text{ jet}]$		$^{+0.5}_{-0.5}$	$^{+7.5}_{-4.8}$	$^{+8.6}_{-8.7}$	$^{+9.0}_{-8.9}$	$^{+10.0}_{-9.3}$	$^{+11.3}_{-11.0}$	$^{+12.5}_{-12.5}$	$^{+4.0}_{-4.4}$
JES $[e^+e^-, 3 \text{ jet}]$		+8.6	$+32.9 \\ -29.5$	$^{+14.6}_{-14.9}$	$^{+16.5}_{-15.2}$	$^{+20.8}_{-20.8}$	$+17.8 \\ -17.9$	$+18.9 \\ -19.0$	$^{+14.6}_{-15.4}$
JES $[\mu^+\mu^-, 2 \text{ jet}]$		$-8.6 \\ +2.5 \\ -2.5$	$^{+4.5}_{-3.0}$	+6.7 -6.7	$+10.2 \\ -9.9$	+9.2 -9.3	+7.7 -7.6	+11.5 -11.5	+3.9 -4.3
JES $[\mu^+\mu^-, 3 \text{ jet}]$		$+9.2 \\ -9.2$	$^{+13.4}_{-10.4}$	$+14.1 \\ -14.1$	$^{+16.6}_{-16.6}$	$^{+14.7}_{-14.7}$	$+16.8 \\ -16.9$	$+17.5 \\ -17.5$	$^{+11.6}_{-12.2}$
Tight b-tag Rate		0.2	10.4	14.1	10.0	14.1	10.5	11.0	12.2
Loose b-tag Rate		6.3	6.3	6.3	6.3	6.3	6.3		6.3
$t\bar{t}$ Cross Section		10							
Diboson Cross Section			6	6	6				
Z+HF Cross Section						40	40		
ZH Cross Section									5
ISR/FSR									3.1 - 15.2
Electron Trigger Eff.		1	1	1	1	1	1		1
Muon Trigger Eff.		5	5	5	5	5	5		5

TABLE IX: Systematic uncertainties on the signal and background contributions for CDF's $H \to W^+W^- \to \ell^\pm \ell'^\mp$ channels with zero, one, and two or more associated jets. These channels are sensitive to gluon fusion production (all channels) and WH, ZH and VBF production. Systematic uncertainties are listed by name (see the original references for a detailed explanation of their meaning and on how they are derived). Systematic uncertainties for H shown in this table are obtained for $m_H = 160$ GeV/ c^2 . Uncertainties are relative, in percent, and are symmetric unless otherwise indicated. The uncertainties associated with the different background and signal processed are correlated within individual jet categories unless otherwise noted. Boldface and italics indicate groups of uncertainties which are correlated with each other but not the others on the line.

CDF: $H \to W^+W^- \to \ell^{\pm}\ell^{\mp}$ with no associated jet channel relative uncertainties (%)

Contribution	WW	WZ	ZZ	$t ar{t}$	DY	$W\gamma$	W+jet	$gg \to H$	WH	ZH	VBF
Cross Section						,		00			
ScaleInclusive								13.4%			
Scale1+Jets								-23.0%			
Scale2+Jets								0.0%			
PDF Model								7.6%			
Total	6.0%	6.0%	6.0%	7.0%					5.0%	5.0%	10.0%
Acceptance											
Scale (jets)	$0.3\% \mathrm{s}$										
PDF Model (leptons)								2.7%			
PDF Model (jets)	1.1%							5.5%			
Higher-order Diagrams		10.0%	10.0%	10.0%		10.0%			10.0%	10.0%	10.0%
$E_T Modeling$					19.0%						
Conversion Modeling						6.8%					
Jet Fake Rates											
(Low S/B)							15.0%				
(High S/B)							24.0%				
Jet Energy Scale	3.1%	6.2%	3.5%	28.2%	18.0%	3.5%		5.7%	9.9%	5.3%	12.9%
Lepton ID Efficiencies	3.8%	3.8%	3.8%	3.8%	3.8%			3.8%	3.8%	3.8%	3.8%
Trigger Efficiencies	2.0%	2.0%	2.0%	2.0%	2.0%			2.0%	2.0%	2.0%	2.0%
Luminosity	5.9%	5.9%	5.9%	5.9%	5.9%			5.9%	5.9%	5.9%	5.9%

CDF: $H \to W^+W^- \to \ell^{\pm}\ell'^{\mp}$ with one associated jet channel relative uncertainties (%)

Contribution	WW	WZ	ZZ	$t \bar t$	DY	$W\gamma$	W+jet	$gg \to H$	WH	ZH	VBF
Cross Section											
ScaleInclusive								0.0%			
Scale1+Jets								35.0%			
Scale2+Jets								-12.7%			
PDF Model								17.3%			
Total	6.0%	6.0%	6.0%	7.0%					5.0%	5.0%	10.0%
Acceptance											
Scale (jets)	-4.0%s										
PDF Model (leptons)								3.6%			
PDF Model (jets)	4.7%							-6.3%			
Higher-order Diagrams		10.0%	10.0%	10.0%		10.0%			10.0%	10.0%	10.0%
$E_T Modeling$					21.0%						
Conversion Modeling						6.8%					
Jet Fake Rates											
(Low S/B)							16.0%				
(High S/B)							27.0%				
Jet Energy Scale	-5.8%	-1.1%	-4.8%	-13.1%	-6.5%	-9.5%		-3.8%	-8.5%	-7.8%	-6.8%
Lepton ID Efficiencies	3.8%	3.8%	3.8%	3.8%	3.8%			3.8%	3.8%	3.8%	3.8%
Trigger Efficiencies	2.0%	2.0%	2.0%	2.0%	2.0%			2.0%	2.0%	2.0%	2.0%
Luminosity	5.9%	5.9%	5.9%	5.9%	5.9%			5.9%	5.9%	5.9%	5.9%

CDF: $H \to W^+W^- \to \ell^{\pm}\ell'^{\mp}$ with two or more associated jets channel relative uncertainties (%)

Contribution	WW	WZ	ZZ	t ar t	DY	$W\gamma$	W+jet	$gg \to H$	WH	ZH	VBF
Cross Section											
ScaleInclusive								0.0%			
Scale1+Jets								0.0%			
Scale2+Jets								33.0%			
PDF Model								29.7%			
Total	6.0%	6.0%	6.0%	7.0%					5.0%	5.0%	10.0%
Acceptance											
Scale (jets)	-8.2%s										
PDF Model (leptons)								4.8%			
PDF Model (jets)	4.2%							-12.3%			
Higher-order Diagrams		10.0%	10.0%	10.0%		10.0%			10.0%	10.0%	10.0%
$E_T \!$					26.0%						
Conversion Modeling						6.8%					
Jet Fake Rates							19.0%				
Jet Energy Scale	-20.5%	-13.2%	-13.3%	-1.7%	-32.7%	-22.0%		-15.1%	-4.0%	-2.5%	-3.8%
b-tag Veto				3.6%							
Lepton ID Efficiencies	3.8%	3.8%	3.8%	3.8%	3.8%			3.8%	3.8%	3.8%	3.8%
Trigger Efficiencies	2.0%	2.0%	2.0%	2.0%	2.0%			2.0%	2.0%	2.0%	2.0%
Luminosity	5.9%	5.9%	5.9%	5.9%	5.9%			5.9%	5.9%	5.9%	5.9%

TABLE X: Systematic uncertainties on the signal and background contributions for CDF's low- $M_{\ell\ell}$ $H \to W^+W^- \to \ell^\pm \ell'^\mp$ channel with zero or one associated jets. This channel is sensitive to only gluon fusion production. Systematic uncertainties are listed by name (see the original references for a detailed explanation of their meaning and on how they are derived). Systematic uncertainties for H shown in this table are obtained for $m_H = 160~{\rm GeV}/c^2$. Uncertainties are relative, in percent, and are symmetric unless otherwise indicated. The uncertainties associated with the different background and signal processed are correlated within individual categories unless otherwise noted. In these special cases, the correlated uncertainties are shown in either italics or bold face text.

CDF: low $M_{\ell\ell}$ $H \to W^+W^- \to \ell^{\pm}\ell'^{\mp}$ with zero or one associated jets channel relative uncertainties (%)

Contribution	WW	WZ	ZZ	$t ar{t}$	DY	$W\gamma$	W+jet(s)	$gg \to H$	WH	ZH	VBF
Cross Section							- , ,				
ScaleInclusive								8.1%			
Scale1+Jets								0.0%			
Scale2+Jets								-5.1%			
PDF Model								10.5%			
Total	6.0%	6.0%	6.0%	7.0%	5.0%				5.0%	5.0%	10.0%
Acceptance											
Scale (jets)	-0.4%s										
PDF Model (leptons)								1.0%			
PDF Model (jets)	1.6%							2.1%			
Higher-order Diagrams		10.0%	10.0%	10.0%	10.0%				10.0%	10.0%	10.0%
Conversion Modeling						8.4%					
Jet Fake Rates							13.8%				
Jet Energy Scale	1.2%	2.2%	2.0%	13.3%	15.4%	1.2%		2.4%	9.2%	6.5%	7.8%
Lepton ID Efficiencies	3.8%	3.8%	3.8%	3.8%	3.8%			3.8%	3.8%	3.8%	3.8%
Trigger Efficiencies	2.0%	2.0%	2.0%	2.0%	2.0%			2.0%	2.0%	2.0%	2.0%
Luminosity	5.9%	5.9%	5.9%	5.9%	5.9%			5.9%	5.9%	5.9%	5.9%

TABLE XI: Systematic uncertainties on the signal and background contributions for CDF's $H \to W^+W^- \to e^\pm \tau^\mp$ and $H \to W^+W^- \to \mu^\pm \tau^\mp$ channels. These channels are sensitive to gluon fusion production, WH, ZH and VBF production. Systematic uncertainties are listed by name (see the original references for a detailed explanation of their meaning and on how they are derived). Systematic uncertainties for H shown in this table are obtained for $m_H = 160 \text{ GeV}/c^2$. Uncertainties are relative, in percent, and are symmetric unless otherwise indicated. The uncertainties associated with the different background and signal processed are correlated within individual categories unless otherwise noted. In these special cases, the correlated uncertainties are shown in either italics or bold face text.

CDF: $H \to W^+W^- \to e^{\pm}\tau^{\mp}$ channel relative uncertainties ()

Contribution	WW	WZ	ZZ	$t \bar t$	$Z \to \tau\tau$	$Z \to \ell \ell$	$W+\mathrm{jet}$	$W\gamma$	$gg \to H$	WH	ZH	VBF
Cross section	6.0	6.0	6.0	10.0	5.0	5.0			10.3	5	5	10
Measured W cross-section							12					
PDF Model	1.6	2.3	3.2	2.3	2.7	4.6	2.2	3.1	2.5	2.0	1.9	1.8
Higher order diagrams	10	10	10	10	10	10		10		10	10	10
Conversion modeling								10				
Trigger Efficiency	0.5	0.6	0.6	0.6	0.7	0.5	0.6	0.6	0.5	0.5	0.6	0.5
Lepton ID Efficiency	0.4	0.5	0.5	0.4	0.4	0.4	0.5	0.4	0.4	0.4	0.4	0.4
τ ID Efficiency	1.0	1.3	1.9	1.3	2.1			0.3	2.8	1.6	1.7	2.8
Jet into τ Fake rate	5.8	4.8	2.0	5.1		0.1	8.8			4.2	4.0	0.4
Lepton into τ Fake rate	0.2	0.1	0.6	0.2		2.3		2.1	0.15	0.06	0.15	0.11
W+jet scale							1.6					
MC Run dependence	2.6	2.6	2.6				2.6					
Luminosity	3.8	3.8	3.8	3.8	3.8	3.8	3.8	3.8	3.8	3.8	3.8	3.8
Luminosity Monitor	4.4	4.4	4.4	4.4	4.4	4.4	4.4	4.4	4.4	4.4	4.4	4.4

CDF: $H \to W^+W^- \to \mu^{\pm}\tau^{\mp}$ channel relative uncertainties (%)

Contribution	WW	WZ	ZZ	t ar t	$Z \to au au$	$Z \to \ell \ell$	W+jet	$W\gamma$	$gg \to H$	WH	ZH	VBF
Cross section	6.0	6.0	6.0	10.0	5.0	5.0			10.4	5	5	10
Measured W cross-section							12					
PDF Model	1.5	2.1	2.9	2.1	2.5	4.3	2.0	2.9	2.6	2.2	2.0	2.2
Higher order diagrams	10	10	10	10				11		10	10	10
Trigger Efficiency	1.3	0.7	0.7	1.1	0.9	1.3	1.0	1.0	1.3	1.3	1.2	1.3
Lepton ID Efficiency	1.1	1.4	1.4	1.1	1.2	1.1	1.4	1.3	1.0	1.0	1.0	1.0
τ ID Efficiency	1.0	1.2	1.4	1.6	1.9				2.9	1.6	1.7	2.8
Jet into τ Fake rate	5.8	5.0	4.4	4.4		0.2	8.8			4.5	4.2	0.4
Lepton into τ Fake rate	0.06	0.05	0.09	0.04		1.9		1.2	0.04	0.02	0.02	0.04
W+jet scale							1.4					
MC Run dependence	3.0	3.0	3.0				3.0					
Luminosity	3.8	3.8	3.8	3.8	3.8	3.8	3.8	3.8	3.8	3.8	3.8	3.8
Luminosity Monitor	4.4	4.4	4.4	4.4	4.4	4.4	4.4	4.4	4.4	4.4	4.4	4.4

TABLE XII: Systematic uncertainties on the signal and background contributions for CDF's $WH \to WWW \to \ell^{\pm}\ell'^{\pm}$ channel with one or more associated jets and $WH \to WWW \to \ell^{\pm}\ell'^{\pm}\ell''^{\mp}$ channel. These channels are sensitive to only WH and ZH production. Systematic uncertainties are listed by name (see the original references for a detailed explanation of their meaning and on how they are derived). Systematic uncertainties for H shown in this table are obtained for $m_H = 160 \text{ GeV}/c^2$. Uncertainties are relative, in percent, and are symmetric unless otherwise indicated. The uncertainties associated with the different background and signal processed are correlated within individual categories unless otherwise noted. In these special cases, the correlated uncertainties are shown in either italics or bold face text.

CDF: $WH \to WWW \to \ell^{\pm}\ell'^{\pm}$ channel relative uncertainties (%)

Contribution	WW	WZ	ZZ	$t \bar{t}$	DY	$W\gamma$	$W+\mathrm{jet}$	WH	ZH
Cross Section							,, ,,,,,,		
Total	6.0%	6.0%	6.0%	7.0%	5.0%			5.0%	5.0%
Acceptance									
Scale (jets)	-6.1%								
PDF Model (jets)	5.7%								
Higher-order Diagrams		10.0%	10.0%	10.0%	10.0%	10.0%		10.0%	10.0%
Conversion Modeling						6.8%			
Jet Fake Rates							37.7%		
Charge Mismeasurement Rate	25.0%				25.0%				
Jet Energy Scale	-4.1%	-4.2% s	-3.3%s	-0.3%	-4.9%s	-9.1%		-1.0%s	-0.7%s
Lepton ID Efficiencies	3.8%	3.8%	3.8%	3.8%	3.8%			3.8%	3.8%
Trigger Efficiencies	2.0%	2.0%	2.0%	2.0%	2.0%			2.0%	2.0%
Luminosity	5.9%	5.9%	5.9%	5.9%	5.9%			5.9%	5.9%

CDF: $WH \to WWW \to \ell^{\pm} \ell'^{\pm} \ell''^{\mp}$ channel relative uncertainties (%)

Contribution	WZ	ZZ	$Z\gamma$	$t ar{t}$	Fakes	WH	ZH
Cross Section							
Total	6.0%	6.0%	10.0%	7.0%		5.0%	5.0%
Acceptance							
Higher-order Diagrams	10.0%	10.0%	15.0%	10.0%		10.0%	10.0%
Jet Fake Rates					22.3%		
b-Jet Fake Rates				27.3%			
Jet Energy Scale			-3.0%				
Lepton ID Efficiencies	5.0%	5.0%	5.0%	5.0%		5.0%	5.0%
Trigger Efficiencies	2.0%	2.0%	2.0%	2.0%		2.0%	2.0%
Luminosity	5.9%	5.9%	5.9%	5.9%		5.9%	5.9%

TABLE XIII: Systematic uncertainties on the signal and background contributions for CDF's $ZH \to ZWW \to \ell^{\pm}\ell^{\mp}\ell'^{\pm}$ channels with 1 jet and 2 or more jets. These channels are sensitive to only WH and ZH production. Systematic uncertainties are listed by name (see the original references for a detailed explanation of their meaning and on how they are derived). Systematic uncertainties for H shown in this table are obtained for $m_H = 160 \text{ GeV}/c^2$. Uncertainties are relative, in percent, and are symmetric unless otherwise indicated. The uncertainties associated with the different background and signal processed are correlated within individual categories unless otherwise noted. In these special cases, the correlated uncertainties are shown in either italics or bold face text.

CDF: $ZH \to ZWW \to \ell^{\pm}\ell^{\mp}\ell'^{\pm}$ with one associated jet channel relative uncertainties (%)

Contribution	WZ	ZZ	$Z\gamma$	$t ar{t}$	Fakes	WH	ZH
Cross Section							
Total	6.0%	6.0%	10.0%	7.0%		5.0%	5.0%
Acceptance							
Higher-order Diagrams	10.0%	10.0%	15.0%	10.0%		10.0%	10.0%
Jet Fake Rates					23.6%		
b-Jet Fake Rates				42.0%			
Jet Energy Scale	-7.8%	-2.4%	-6.4%	2.2%		-7.0%	7.1%
Lepton ID Efficiencies	5.0%	5.0%	5.0%	5.0%		5.0%	5.0%
Trigger Efficiencies	2.0%	2.0%	2.0%	2.0%		2.0%	2.0%
Luminosity	5.9%	5.9%	5.9%	5.9%		5.9%	5.9%

CDF: $ZH \to ZWW \to \ell^{\pm}\ell^{\mp}\ell'^{\pm}$ with two or more associated jets channel relative uncertainties (%)

Contribution	WZ	ZZ	$Z\gamma$	$tar{t}$	Fakes	WH	ZH
Cross Section							
Total	6.0%	6.0%	10.0%	7.0%		5.0%	5.0%
Acceptance							
Higher-order Diagrams	10.0%	10.0%	15.0%	10.0%		10.0%	10.0%
Jet Fake Rates					18.4%		
b-Jet Fake Rates				22.2%			
Jet Energy Scale	-18.0%	-15.4%	-16.8%	-2.3%		-20.1%	-5.5%
Lepton ID Efficiencies	5.0%	5.0%	5.0%	5.0%		5.0%	5.0%
Trigger Efficiencies	2.0%	2.0%	2.0%	2.0%		2.0%	2.0%
Luminosity	5.9%	5.9%	5.9%	5.9%		5.9%	5.9%

TABLE XIV: Systematic uncertainties on the signal and background contributions for CDF's $H \to \ell^{\pm}\ell^{\mp}\ell^{\prime\pm}\ell^{\prime\mp}$ channel. This channel is sensitive to gluon fusion production and WH, ZH and VBF production. Systematic uncertainties are listed by name (see the original references for a detailed explanation of their meaning and on how they are derived). Uncertainties are relative, in percent, and are symmetric unless otherwise indicated. The uncertainties associated with the different background and signal processed are correlated unless otherwise noted. Boldface and italics indicate groups of uncertainties which are correlated with each other but not the others within a line. Shape uncertainties are labeled with an "s".

CDF: $H \to \ell^{\pm} \ell^{\prime \pm} \ell^{\prime \pm}$ channel relative uncertainties (%)

Contribution	ZZ	$Z(/\gamma^*)$ +jets	gg o H	WH	ZH	VBF
	ZZ	Z(/'y)+jets	$gg \rightarrow II$	VV 11	Z11	VDF
Cross Section:						
Scale			7.0			
PDF Model			7.7			
Total	10.0			5.0	5.0	10.0
$\mathcal{BR}(H \to VV)$			3.0	3.0	3.0	3.0
Acceptance:						
PDF Model	2.7					
Higher-order Diagrams	2.5					
Jet Fake Rates		50.0				
$\not\!\!E_T$ Resolution	S		S		S	S
Lepton ID Efficiencies	3.6		3.6	3.6	3.6	3.6
Trigger Efficiencies	0.4		0.5	0.5	0.5	0.5
Luminosity	5.9		5.9	5.9	5.9	5.9

TABLE XV: Systematic uncertainties on the signal and background contributions for CDF's $t\bar{t}H \to \ell + jets$ channels. Systematic uncertainties are listed by name; see the original references for a detailed explanation of their meaning and on how they are derived. Systematic uncertainties for $t\bar{t}H$ shown in this table are obtained for $m_H = 115 \text{ GeV}/c^2$. Uncertainties are relative, in percent, and are symmetric unless otherwise indicated.

CDF: $t\bar{t}H \ell + \not\!\!E_T + 4$ jets relative uncertainties (%)

	1 tight.	, 1 loose	1 tight,	≥ 2 loose	2 tight,	0 loose	2 tight,	≥ 1 loose	≥ 3 tight,	≥ 0 loose
Contribution	$t \bar t$	$t \bar{t} H$	t ar t	$t \bar{t} H$	$t \bar{t}$	$t\bar{t}H$	t ar t	$t \bar{t} H$	$t \bar{t}$	$t\bar{t}H$
$t\bar{t}$ Cross Section		10		10		10		10		10
$t\bar{t}H$ Cross Section	10		10		10		10		10	
Luminosity $(\sigma_{\rm inel}(p\bar{p}))$	3.8	3.8	3.8	3.8	3.8	3.8	3.8	3.8	3.8	3.8
Luminosity Monitor	4.4	4.4	4.4	4.4	4.4	4.4	4.4	4.4	4.4	4.4
B-Tag Efficiency	$^{+1.4}_{-2.5}$	$-2.9 \\ -2.0$	$^{+3.3}_{-1.5}$	$^{+0.3}_{+0.3}$	$^{+7.3}_{-9.4}$	$^{+6.7}_{-2.0}$	$^{+8.3}_{-8.8}$	$^{+7.0}_{-7.7}$	$^{+11}_{-12}$	$^{+11}_{-16}$
Mistag Rate	$^{+1.7}_{-2.0}$	$-0.4 \\ -1.5$	$^{+10}_{-11}$	$^{-1.1}_{-5.7}$	$^{-1.2}_{+2.7}$	$^{+2.7}_{+3.7}$	$^{+7.6}_{-7.4}$	$^{+1.7}_{+2.4}$	$^{+3.3}_{-5.1}$	$^{+1.6}_{+0.2}$
Jet Energy Scale	$^{+3.8}_{-5.1}$	$^{-13}_{+6.7}$	$^{+2.5}_{-4.5}$	0.0 0.0	$^{+4.2}_{-4.8}$	$-5.9 \\ +5.9$	$^{+2.5}_{-3.8}$	$-12 \\ 0.0$	$^{+3.3}_{-4.4}$	$-12 \\ 0.0$
ISR+FSR+PDF	$^{-1.8}_{-1.0}$	$^{-0.1}_{+0.1}$	$^{-1.3}_{+2.3}$	$-0.5 \\ +0.5$	$-3.8 \\ -1.3$	$^{+0.2}_{-0.2}$	$-4.4 \\ -1.1$	$^{+0.0}_{-0.0}$	$-2.9 \\ -3.5$	$^{-0.2}_{+0.2}$

CDF: $t\bar{t}H$ $\ell + \not\!\!E_T + 5$ jets relative uncertainties (%)

	1 tight	, 1 loose	1 tight,	≥ 2 loose	2 tight	, 0 loose	2 tight,	≥ 1 loose	≥ 3 tight	0 loose
Contribution	$t \bar t$	$t\bar{t}H$	t ar t	$t\bar{t}H$	$t\bar{t}$	$t\bar{t}H$	$t\bar{t}$	$t\bar{t}H$	$t\bar{t}$	$t\bar{t}H$
$t\bar{t}$ Cross Section		10		10		10		10		10
$t\bar{t}H$ Cross Section	10		10		10		10		10	
Luminosity $(\sigma_{\text{inel}}(p\bar{p}))$	3.8	3.8	3.8	3.8	3.8	3.8	3.8	3.8	3.8	3.8
Luminosity Monitor	4.4	4.4	4.4	4.4	4.4	4.4	4.4	4.4	4.4	4.4
B-Tag Efficiency	$^{+1.8}_{-3.5}$	$^{-0.4}_{+2.7}$	$^{+4.5}_{-4.1}$	$-1.3 \\ -1.6$	$^{+8.2}_{-6.8}$	$^{+2.5}_{-5.0}$	$^{+9.7}_{-7.7}$	$^{+5.9}_{-5.5}$	$^{+11}_{-16}$	$^{+9.9}_{-13}$
Mistag Rate	$^{+1.3}_{-2.9}$	$-7.5 \\ +1.8$	$^{+18}_{-8.9}$	$^{+4.3}_{-6.6}$	$^{-0.2}_{+2.6}$	$^{-2.0}_{+1.0}$	$^{+8.2}_{-8.7}$	$^{+2.5}_{-2.2}$	$^{+8.1}_{-3.4}$	$^{+1.3}_{-0.5}$
Jet Energy Scale	$^{+19}_{-16}$	$^{+7.5}_{-7.5}$	$^{+17}_{-15}$	$^{+7.1}_{-14}$	$^{+18}_{-17}$	$^{+7.0}_{-4.7}$	$^{+16}_{-16}$	$^{+6.7}_{-3.3}$	$^{+15}_{-15}$	$-2.7 \\ -8.1$
ISR+FSR+PDF	$^{+10}_{-1.2}$	$^{-0.0}_{+0.0}$	$^{+14}_{-1.0}$	$^{-0.2}_{+0.2}$	$^{+8.2}_{-6.5}$	$^{+0.0}_{-0.0}$	$^{+12}_{-5.1}$	$^{-2.1}_{+2.1}$	$^{+14}_{-2.0}$	$^{-1.9}_{+1.9}$

TABLE XVI: Systematic uncertainties on the signal and background contributions for CDF's $t\bar{t}H$ 2-tag and 3-tag \rlap/E_T +jets channels. Systematic uncertainties are listed by name; see the original references for a detailed explanation of their meaning and on how they are derived. Systematic uncertainties for $t\bar{t}H$ shown in this table are obtained for $m_H=120~{\rm GeV}/c^2$. Uncertainties are relative, in percent, and are symmetric unless otherwise indicated.

CDF: $t\bar{t}H \not E_T$ +jets 2-tag channel relative uncertainties (%)

Contribution	non- $tar{t}$	t ar t	$t \bar{t} H$
Luminosity $(\sigma_{\text{inel}}(p\bar{p}))$	0	3.8	3.8
Luminosity Monitor	0	4.4	4.4
Jet Energy Scale	0	2	11
Trigger Efficiency	0	7	7
B-Tag Efficiency	0	7	7
ISR/FSR	0	2	2
PDF	0	2	2
$t\bar{t}$ Cross Section	0	10	0
$t\bar{t}b\bar{b}$ Cross Section	0	3	0
Signal Cross Section	0	0	10
Background Modeling	6	0	0
Background B-tagging	5	0	0

CDF: $t\bar{t}H \not \!\! E_T$ +jets 3-tag channel relative uncertainties (%)

Contribution	non- $tar{t}$	$tar{t}$	t ar t H
Luminosity $(\sigma_{\text{inel}}(p\bar{p}))$	0	3.8	3.8
Luminosity Monitor	0	4.4	4.4
Jet Energy Scale	0	3	13
Trigger Efficiency	0	7	7
B-Tag Efficiency	0	9	9
ISR/FSR	0	2	2
PDF	0	2	2
$t\bar{t}$ Cross Section	0	10	0
$t\bar{t}b\bar{b}$ Cross Section	0	5	0
Signal Cross Section	0	0	10
Background Modeling	6	0	0
Background B -tagging	10	0	0

TABLE XVII: Systematic uncertainties on the signal and background contributions for CDF's $t\bar{t}H$ 2-tag and 3-tag all jets channels. Systematic uncertainties are listed by name; see the original references for a detailed explanation of their meaning and on how they are derived. Systematic uncertainties for $t\bar{t}H$ shown in this table are obtained for $m_H = 120~{\rm GeV}/c^2$. Uncertainties are relative, in percent, and are symmetric unless otherwise indicated.

CDF: $t\bar{t}H$ all jets 2-tag channel relative uncertainties (%)

Contribution	non- $tar{t}$	t ar t	$t \bar{t} H$
Luminosity $(\sigma_{\text{inel}}(p\bar{p}))$	0	3.8	3.8
Luminosity Monitor	0	4.4	4.4
Jet Energy Scale	0	11	20
Trigger Efficiency	0	7	7
B-Tag Efficiency	0	7	7
ISR/FSR	0	2	2
PDF	0	2	2
$t\bar{t}$ Cross Section	0	10	0
$t\bar{t}b\bar{b}$ Cross Section	0	3	0
Signal Cross Section	0	0	10
Background Modeling	9	0	0
Background B-tagging	5	0	0

CDF: $t\bar{t}H$ all jets 3-tag channel relative uncertainties (%)

Contribution	non- $tar{t}$	t ar t	t ar t H
Luminosity $(\sigma_{\text{inel}}(p\bar{p}))$	0	3.8	3.8
Luminosity Monitor	0	4.4	4.4
Jet Energy Scale	0	13	22
Trigger Efficiency	0	7	7
B-Tag Efficiency	0	9	9
ISR/FSR	0	2	2
PDF	0	2	2
$t\bar{t}$ Cross Section	0	10	0
$t\bar{t}b\bar{b}$ Cross Section	0	6	0
Signal Cross Section	0	0	10
Background Modeling	9	0	0
Background B-tagging	10	0	0

TABLE XVIII: Systematic uncertainties on the signal and background contributions for CDF's $H \to \tau^+ \tau^-$ channels. Systematic uncertainties are listed by name; see the original references for a detailed explanation of their meaning and on how they are derived. Systematic uncertainties for the Higgs signal shown in these tables are obtained for $m_H = 120 \text{ GeV}/c^2$. Uncertainties are relative, in percent, and are symmetric unless otherwise indicated. Shape uncertainties are labeled with an "S".

CDF: $H \to \tau^+ \tau^- (e/\mu + \tau_{had})$ channel relative uncertainties (%)

	7 / *	5 / *	5 / *	. =			***				
Contribution	$Z/\gamma^* \to \tau\tau$	$Z/\gamma^* \to ee$	$Z/\gamma^* \to \mu\mu$	tt	diboson	fakes from SS	W+jets	WH	ZH	VBF	$gg \rightarrow H$
PDF Uncertainty	-	-	-	-	-	-	-	1.2	0.9	2.2	4.9
ISR/FSR 1 JET	-	-	-	-	-	-	-	6.7	8.7	8.8	3.6
$ISR/FSR \ge 2 JETS$	-	-	-	-	-	-	-	4.8	3.8	3.9	19.1
JES (S) 1 JET	9.5	8.5	8.5	14.5	0.5	-	4.2	2.8	6.4	6.5	4.3
$JES(S) \ge 2 JETS$	18.9	22.3	22.3	1.3	10.7	-	15.4	5.1	3.9	3.7	14.5
Normalization 1 JET	2.0	5.0	5.0	10.0	6.0	1.3	14.8	5.0	5.0	10.0	23.5
Normalization ≥ 2 JETS	2.0	5.0	5.0	10.0	6.0	2.5	14.8	5.0	5.0	10.0	33.0
ε_{trig} (e leg)	0.3	0.3	-	0.3	0.3	-	-	0.3	0.3	0.3	0.3
$\varepsilon_{trig} \ (\mu \ \mathrm{leg})$	1.0	-	1.0	1.0	1.0	-	-	1.0	1.0	1.0	1.0
$\varepsilon_{trig} \ (\tau \ \mathrm{leg})$	3.0	3.0	3.0	3.0	3.0	-	-	3.0	3.0	3.0	3.0
$arepsilon_{ID}e$	2.4	2.4	-	2.4	2.4	_	-	2.4	2.4	2.4	2.4
$arepsilon_{ID}\mu$	2.6	-	2.6	2.6	2.6	-	-	2.6	2.6	2.6	2.6
$arepsilon_{ID} au$	3.0	3.0	3.0	3.0	3.0	-	-	3.0	3.0	3.0	3.0
$arepsilon_{vtx}$	0.5	0.5	0.5	0.5	0.5	-	-	0.5	0.5	0.5	0.5
Luminosity	5.9	5.9	5.9	5.9	5.9	-	-	5.9	5.9	5.9	5.9

TABLE XIX: Systematic uncertainties on the signal and background contributions for CDF's $WH \to \ell\nu\tau^+\tau^-$ and $ZH \to \ell^+\ell^-\tau^+\tau^-$ channels. Systematic uncertainties are listed by name; see the original references for a detailed explanation of their meaning and on how they are derived. Systematic uncertainties for the Higgs signal shown in these tables are obtained for $m_H = 120~{\rm GeV}/c^2$. Uncertainties are relative, in percent, and are symmetric unless otherwise indicated.

CDF: $WH \to \ell\nu\tau^+\tau^-$ and $ZH \to \ell^+\ell^-\tau^+\tau^ \ell\ell\tau_h + X$ channel relative uncertainties (%)

Contribution	ZZ	WZ	WW	DY(ee)	$DY(\mu\mu)$	$DY(\tau\tau)$	$Z\gamma$	$t \bar t$	$W\gamma$	W + jet	WH	ZH	VBF	$gg \to H$
Luminosity	5.9	5.9	5.9	5.9	5.9	5.9	5.9	5.9	5.9	5.9	5.9	5.9	5.9	5.9
Cross Section	11.7	11.7	11.7	5.0	5.0	5.0	11.7	14.1	11.7	5.0	5.0	5.0	10.0	10.0
Z-vertex Cut Efficiency	0.5	0.5	0.5	0.5	0.5	0.5	0.5	0.5	0.5	0.5	0.5	0.5	0.5	0.5
Trigger Efficiency	1.1	1.1	1.0	1.0	1.0	1.1	1.1	1.0	0.8	1.0	1.2	1.2	1.2	1.1
Lepton ID Efficiency	2.4	2.3	2.4	2.4	2.4	2.4	2.4	2.4	2.3	2.4	2.4	2.4	2.4	2.4
Lepton Fake Rate	10.7	8.0	26.7	26.0	26.6	15.1	27.1	22.4	22.8	28.7	2.9	2.3	15.1	13.6
Jet Energy Scale	1.3	1.1	0.0	3.2	5.1	0.6	6.6	0.1	2.0	0.2	0.1	0.03	0.6	0.4
MC stat	3.7	2.9	7.6	1.5	1.7	2.2	4.1	3.1	20.0	3.1	1.5	1.4	3.8	9.4
PDF Model	-	-	-	-	-	-	-	-	-	-	1.2	0.9	2.2	4.9
ISR/FSR Uncertainties	-	-	-	-	-	-	-	-	-	-	1.3	2.1	0.6	0.2

CDF: $WH \to \ell\nu\tau^+\tau^-$ and $ZH \to \ell^+\ell^-\tau^+\tau^ e\mu\tau_h + X$ channel relative uncertainties (%)

Contribution	ZZ	WZ	WW	DY(ee)	$DY(\mu\mu)$	$DY(\tau\tau)$	$Z\gamma$	$t \bar t$	$W\gamma$	W + jet	WH	ZH	VBF	$gg \to H$
Luminosity	5.9	5.9	5.9	5.9	5.9	5.9	5.9	5.9	5.9	5.9	5.9	5.9	5.9	5.9
Cross Section	11.7	11.7	11.7	5.0	5.0	5.0	11.7	14.1	11.7	5.0	5.0	5.0	10.0	10.0
Z-vertex Cut Efficiency	0.5	0.5	0.5	0.5	0.5	0.5	0.5	0.5	0.5	0.5	0.5	0.5	0.5	0.5
Trigger Efficiency	1.4	1.4	1.1	1.1	1.3	1.1	1.4	1.1	1.0	0.7	1.3	1.3	1.2	1.2
Lepton ID Efficiency	2.4	2.4	2.4	2.4	2.4	2.4	2.4	2.4	2.4	2.4	2.4	2.4	2.4	2.4
Lepton Fake Rate	9.0	6.5	26.6	20.8	31.4	25.2	39.4	27.8	19.3	41.9	1.6	2.5	28.5	29.2
Jet Energy Scale	0.0	0.3	2.2	0.0	0.8	1.5	0.5	0.8	0.0	0.0	0.2	0.1	1.7	0.0
MC stat	12.9	7.2	20.9	57.7	12.6	7.7	10.2	12.4	35.4	25.8	2.1	3.9	13.0	44.7
PDF Model	-	-	-	-	-	-	-	-	-	-	1.2	0.9	2.2	4.9
ISR/FSR Uncertainties	-	-	-	-	-	-	-	-	-	-	0.6	0.2	0.1	0.0

CDF: $WH \to \ell\nu\tau^+\tau^-$ and $ZH \to \ell^+\ell^-\tau^+\tau^ \ell\tau_h\tau_h + X$ channel relative uncertainties (%)

Contribution	ZZ	WZ	WW	DY(ee)	$DY(\mu\mu)$	$DY(\tau\tau)$	$Z\gamma$	$t\bar{t}$	$W\gamma$	W + jet	WH	ZH	VBF	$gg \to H$
Luminosity	5.9	5.9	5.9	5.9	5.9	5.9	5.9	5.9	5.9	5.9	5.9	5.9	5.9	5.9
Cross Section	11.7	11.7	11.7	5.0	5.0	5.0	11.7	14.1	11.7	5.0	5.0	5.0	10.0	10.0
Z-vertex Cut Efficiency	0.5	0.5	0.5	0.5	0.5	0.5	0.5	0.5	0.5	0.5	0.5	0.5	0.5	0.5
Trigger Efficiency	1.0	1.1	0.9	1.0	1.1	1.1	1.1	1.0	0.7	0.9	1.1	1.1	1.1	1.1
Lepton ID Efficiency	3.3	3.3	3.3	3.3	3.3	3.3	3.3	3.3	3.3	3.3	3.3	3.3	3.3	3.3
Lepton Fake Rate	10.4	6.8	38.1	43.3	39.9	24.8	32.8	34.2	28.8	34.8	3.1	5.9	28.1	26.3
Jet Energy Scale	5.5	0.0	0.0	3.3	1.6	1.2	1.6	0.0	0.0	1.1	0.1	0.6	1.8	1.7
MC stat	12.5	8.1	16.9	18.3	12.5	4.9	12.6	14.7	70.7	8.7	2.0	3.3	9.4	18.3
PDF Model	-	-	-	-	-	-	-	-	-	-	1.2	0.9	2.2	4.9
ISR/FSR Uncertainties	-	-	-	-	-	-	-	-	-	-	1.2	0.5	0.4	0.04

TABLE XX: Systematic uncertainties on the signal and background contributions for CDF's $WH+ZH \rightarrow jjbb$ and $VBF \rightarrow jjbb$ channels. Systematic uncertainties are listed by name; see the original references for a detailed explanation of their meaning and on how they are derived. Uncertainties with provided shape systematics are labeled with "s". Systematic uncertainties for H shown in this table are obtained for $m_H = 115 \text{ GeV}/c^2$. Uncertainties are relative, in percent, and are symmetric unless otherwise indicated. The cross section uncertainties are uncorrelated with each other (except for single top and $t\bar{t}$, which are treated as correlated). The QCD uncertainty is also uncorrelated with other channels' QCD rate uncertainties.

CDF: $WH +$	$ZH \rightarrow iibb$ and V	$/BF \rightarrow iibb$ channel	relative uncertainties (%)

C	OCD	, , ,		1.1	117/7 . 1 .	3.711	MDD
Contribution	QCD	$t \bar t$	single-top	diboson	W/Z+Jets	VH	VBF
Jet Energy Correction		9 s	9 s	9 s	9 s	9 s	9 s
PDF Modeling						2	2
SecVtx+SecVtx		7.1	7.1	7.1	7.1	7.1	7.1
SecVtx+JetProb		6.4	6.4	6.4	6.4	6.4	6.4
Luminosity		6	6	6	6	6	6
ISR/FSR modeling						3 s	3 s
Jet Width		S	S	S	S	S	S
Trigger		3.6	3.6	3.6	3.6	3.6	3.6
QCD Interpolation	S						
QCD MJJ Tuning	S						
QCD NN Tuning	S						
cross section		7	7	6	50	5	10

TABLE XXI: Systematic uncertainties on the signal and background contributions for CDF's $H \to \gamma \gamma$ channels. Systematic uncertainties are listed by name; see the original references for a detailed explanation of their meaning and on how they are derived. Uncertainties are relative, in percent, and are symmetric unless otherwise indicated.

CDF: $H \to \gamma \gamma$ channel relative uncertainties (%)

Channel	CC	CP	C'C	C'P
Signal Uncertainties:				
Luminosity	6	6	6	6
$\sigma_{ggH}/\sigma_{VH}/\sigma_{VBF}$	14/7/5	14/7/5	14/7/5	14/7/5
PDF	5	2	5	2
ISR/FSR	3	4	2	5
Energy Scale	0.2	0.8	0.1	0.8
Trigger Efficiency	1.0	1.3	1.5	6.0
z Vertex	0.07	0.07	0.07	0.07
Conversion ID	_	=	7	7
Detector Material	0.4	3.0	0.2	3.0
Photon/Electron ID	1.0	2.8	1.0	2.6
Run Dependence	3.0	2.5	1.5	2.0
Data/MC Fits	0.4	0.8	1.5	2.0
Background Uncertainties:				
Fit Function	2.8	0.9	6.1	3.3